

GLASGOW CALEDONIAN UNIVERSITY

MEng Group Research Project

MMH723842-24-AB-GLAS

**Design and Implementation of a Photodiode
Array-Based Analogue 2D Sun Sensor**

word count: xxx

by Zac McCaffery, Alexandru Belea,
Sebastian Alexander, William Kong, Nassor Salim,

Date: April 15, 2025

Contents

Abstract	9
1. Acknowledgements	10
2. Introduction	11
2.1. Problem Statement	11
2.2. Aim of the Project	11
2.3. Objectives of the Project	11
3. Literature Review	13
3.1. CubeSat Design	13
3.2. PSD Enabled Sun Sensor	14
3.3. Mechanical Design and Analysis	14
3.4. Photodiode Simulation and Signal Analysis	14
3.5. IoT Communication Enhancement with LEO Satellites	14
4. Methodology	15
4.1. Prototype Development	15
4.1.1. Lifecycle	15
4.1.2. Signal Conditioning Circuitry	21
4.1.3. Enclosure Design 3D print	23
4.2. Data Acquisition System	23
4.2.1. Functional Requirements	23
4.2.2. Design Approach	24
4.2.3. Technical Specifications	25
4.2.4. Testing Strategy	35
4.2.5. Evaluation of design	35
4.3. Renewable Energy Demonstrator Testbench	36
4.4. Software Model	37
4.4.1. Introduction	37
4.4.2. Theory and Concept	37
4.5. Material Analysis and Selection	38
4.5.1. Material Selection and Requirements	38
4.5.2. External Factors	38

4.5.3. Internal Factors	39
4.5.4. PCB Material Selection	40
4.5.5. CubeSat Chassis Material	45
4.5.6. Quality Assurance and Reliability Standards in Space PCB Manufacturing	46
4.6. Thermal Analysis of the PCB	48
4.6.1. Hypothesis	48
4.6.2. Thermal Analysis Parameters	48
4.6.3. Thermal results	49
4.6.4. Finite Analysis Evaluation 1 - Under 200 °C in space	49
4.6.5. Results Evaluation	51
4.7. CubeSat Chassis Design	51
4.7.1. CubeSat Chassis Design 1	52
4.7.2. CubeSat Chassis Design 2	52
5. Results	56
5.1. Sensor Characterization	56
5.2. Amplification Performance	56
5.3. Photodiode Angular Response	57
5.4. Enclosure Effectiveness	57
5.5. Data Acquisition System Evaluation	57
5.6. System Performance Analysis	57
5.6.1. Operational Constraints Identified	57
5.6.2. Environmental Factors Impact	57
5.6.3. System Stability and Repeatability	57
5.6.4. Recommendations for Improvement	57
5.7. Comparative Analysis	57
5.7.1. Breadboard vs. Stripboard Results	57
5.7.2. Iteration Improvements Analysis	57
5.7.3. Performance Against Design Requirements	57
5.7.4. Design Evolution Assessment	57
5.8. System Limitations And Considerations	57
5.8.1. Angle accuracy	58
6. Conclusions	59
7. Future Work	60
Bibliography	61

A. Appendix - DAQ Code	65
A.1. Arduino DAQ full code	65
A.1.1. Arduino C++ Code	65
A.1.2. PC-side Python Serial Receive Script	67
B. Appendix - Software Model Code	74
B.1. Section 1 Title	74
B.1.1. subsectiontitle	74
B.2. Section 2 Title	74
B.2.1. subsectiontitle	74
C. Appendix - Photos of Lab Work	75
C.1. Prototype Images	75
C.1.1. BreadBoard Prototype	75
C.1.2. Building the Prototype	75
C.1.3. Prototype Testing	75
C.1.4. RED testbench	75
C.1.5. Solar Lab Prototype Testing	75
D. Appendix - Material Analysis	85
D.1. Section 1 Title	85
D.1.1. subsectiontitle	85
D.2. Section 2 Title	85
D.2.1. subsectiontitle	85

List of Figures

4.1. Diagram of Photodiode Array with Apertures	16
4.2. Photo Of BreadBoard Prototype	19
4.3. Photo Of Stripboard Prototype	20
4.4. TIA and Post Amplification Circuit in Altium Designer	22
4.5. Signal Noise Analysis, oscilloscope AC coupled	24
4.6. Flowchart Arduino DAQ C++ program	28
4.7. FSM Arduino C++ LOOP	29
4.8. Python Script Flowchart	32
4.9. Mapping of the s-plane onto the z -plane using the bilinear transformation [1, p.130]	34
4.10. Frequency Response of 4-pole Butterworth Low-Pass Filter (Cutoff: 2.0 Hz, Order: 4, Fs: 500 Hz)	35
4.11. FR-4 PCB [2]	41
4.12. Alumina Oxide PCB [3]	42
4.13. PTFE/Teflon sheets [4]	43
4.14. Copper foils [5]	44
4.15. Kapton PCB [6]	44
4.16. PCB model with Parameters applied	49
4.17. Results under 200 °C radiation	50
4.18. Results under –200 °C radiation	51
4.19. Front view of the first CubeSat chassis design	52
4.20. Angular view of the first CubeSat chassis design	52
4.21. Front view of 1U Cubesat Skeleton Chassis	53
4.22. Angular view of 1U Cubesat Skeleton Chassis	53
4.23. Second chassis design without PCBs	54
4.24. Chassis with the aperture	55

List of Tables

4.1.	Electrical Components Used in Amplification Circuit	17
4.2.	Components Used for DAQ System	17
4.3.	S5971 Photodiode Specifications	17
4.4.	Operational Amplifier Specifications	18

List of Equations

1.	DC Offset Voltage at TIA Output Due to Dark Current	18
2.	Total DC Offset After Post-Amplification	18
3.	Transimpedance Amplifier Output Voltage	21
4.	Photocurrent as Function of Optical Power	21
5.	TIA Output with Photodiode Response	21
6.	Secondary Amplification Gain Calculation	22
7.	Amplifier Feedback Resistor Calculation	22
8.	Default ADC Clock Frequency Calculation	25
9.	Optimized ADC Clock Frequency Calculation	25
10.	Default ADC Conversion Time	25
11.	Optimized ADC Conversion Time	25
12.	Total Sampling Time for 4 Channels (Default)	26
13.	Total Sampling Time for 4 Channels (Optimized)	26
14.	Maximum Theoretical Sampling Frequency (Default)	26
15.	Maximum Theoretical Sampling Frequency (Optimized)	26
16.	Actual Limited Sampling Frequency	26
17.	Total Effective Data Rate	26
18.	Frequency Response of 4th-order Butterworth low-pass filter with 2.0 Hz cutoff	34

ADC	Analog to Digital Converter
ADCS	Attitude determination and control system
ATP	Acquisiton, Tracking and Pointing
CCD	Charge-Coupled Device
CSV	Comma Separated Values
CTE	Coefficient of thermal expansion
DAQ	Data Acquisition System
FOV	Filed of View
GSFC	Goddard Space Flight Centre
LEO	Low Earth Orbit
OPS	Optical Position Sensor
PSD	Position Sensitive Detector
PV	Photovoltaic
RED	Renewable Energy Demonstrator
SGP4	Simplified General Perturbations 4
SMPS	Switch-Mode Power Supply
TIA	Transimpedance Amplifier
TLE	Two-line element set
VLC	Visible Light Communication
WSN	Wireless Sensor Networks
SMD	Surface Mount Device
OpAmp	Operational Amplifier
PCB	Printed Circuit Board
PLA	Polyactic Acid
LED	Light Emiting Diode

Abstract

add abstract here

1. Acknowledgements

We would like to express our sincere gratitude to our supervisors, Dr. Roberto Ramirez-Iniguez and Geraint Bevan, for their invaluable guidance and unwavering support throughout this project.

Our appreciation extends to the 3rd Floor EEE Lab Technicians and Dr. Carlos Gamio-Roffe, whose technical expertise and assistance were instrumental in the successful construction of the prototype.

We are particularly grateful to the European Project Semester RED Team members—Nikolay Ivanov Shopov, Stef Hannisse, and Samridhi Gupta—for generously allowing the use of their Renewable Energy Demonstrator as a testbench. Their contribution provided an ideal platform for positioning light sources during the testing phase of this project.

2. Introduction

2.1. Problem Statement

With the ever-increasing commercialization of the space and satellite industry there is a growing need for a cost-effective method of attitude tracking for smaller satellite missions of such as CubeSat as these missions are purpose built for very specific objectives. Whilst the larger commercial satellite missions make use of expensive digital camera systems for tracking purposes, this is not feasible for much smaller CubeSat setups. CubeSats are defined from 1 unit to 12 – where 1U is a 10x10x10 cm satellite. Consequently, there is a demand for a cost-effective and easily implementable attitude tracking system that can provide accurate measurements for CubeSat missions, such as a Position Sensitive Detector (PSD) using photodiodes.

2.2. Aim of the Project

"To investigate and develop a cost-effective and reliable sun sensing solution suitable for Low Earth Orbit (LEO) nanosatellite attitude determination."

2.3. Objectives of the Project

To investigate the design of a sun sensing system for nanosatellites, used in orientation determination, through detection of its relative position to the sun using analogue sensors located on the satellite's body. Our goal is to create a system which balances cost-effectiveness and simplicity. To achieve this, we will create a software model of the analogue sensor(s) to simulate the system's ability to track the sun from various angles in orbit. After which, we aim to build a physical prototype and use a movable light source to simulate the sun's movement, allowing comparison between the real sensor's performance against our simulations. Although the physical prototype will be built using non-space-grade materials, one of the objectives is to look at and analyse materials required for building a space-grade PCB and sensor. For this step, the Mechanical side of the team will perform Printed circuit board (PCB) and aperture device finite analysis using ANSYS to determine resilience to environmental factors such as stress and thermal simulation. The application of signal processing will be explored to provide usable data, filter out

noise, and improve the system's accuracy. This approach aims to develop a cost-effective and reliable, in-house sun sensing solution specifically for nanosatellites operating in Low Earth Orbit. Major Objective points:

- **Conduct literature review:**

- Analyse existing research on sun sensing technologies, with a focus on PSD-based analogue sensors and their applications in nanosatellites.
- Identify current challenges, best practices, and advancements in attitude determination in Low Earth Orbit. Use these insights to guide the design and optimisation of the proposed sun sensing system.

- **Develop software model:**

- Simulate the performance of the PSD-based analogue sun sensor in tracking the sun's position from various angles in Low Earth Orbit.

- **Design and fabrication of physical prototype:**

- Integrate analogue sun sensor components, test and validate its performance under controlled conditions.

- **Compare simulated and experimental results:**

- Establish evaluation methodology between simulated and experimental test results to ensure that topology evaluation is applicable.

- **Optimise sensor topology:**

- Research and evaluate various configurations of analogue sun sensing systems to maximise sun detection accuracy and minimise blind spots.

- **Investigate environmental factors:**

- Evaluate the material requirements of the PCB and aperture device.

- **Implement signal processing algorithms:**

- Investigate the filtering of noise to enhance the signal-to-noise ratio and otherwise ensure the acquisition of usable data for accurate sun position determination.
- Implement data handling which optimises scanning rates and efficiently processes the analogue signal data for real-time attitude determination.

- **Document results and overall cost-effectiveness:**

- Develop criteria for final evaluation of sun sensing systems, on which to base the final presentation of project findings.

3. Literature Review

3.1. CubeSat Design

Puig-Suari, Turner and Ahlgren published an IEEE paper in 2001 with the help of their students at California Polytechnic State University exploring a need for micro satellites for use by universities in an ever-expanding space programme. They provide as a solution a standard satellite form-factor that will bring down the cost of both manufacture and deployment of satellites by smaller entities: the CubeSat. The paper identifies a key component for the success of this form factor a need for a standard CubeSat deployer mechanism which can deploy several satellites safely and develop such a platform, called Poly Picosatellite Orbital Deployer or P-POD. They point out the need and provide microsatellite size and shape of the CubeSat form factor [7]. Sai balaji et al. performed a study using MATLAB simulation of several attitude control algorithms to look at the ability to control a CubeSat of size 1U. They also simulated sensors such as sun sensors, magnetometer, and gyroscope. They concluded that it is possible to operate the satellite using a magnetorquer type actuator and an array of mathematical models and algorithms: it would take 2000 seconds for a 1U satellite to stabilize at 505km, 98° degree attitude in orbit with the methods utilized by them [8]. Incentivised by the rapidly increasing use of LEO, Lopez-Calle and Franco perform a quantitative comparative study on the catastrophic failure of CubeSats and Nanosats from radiation exposure due to the harsh environment of space versus failure due to collisions in the increasingly busy Low Earth Orbit (LEO). The authors concluded that while sustained damage and damage protection from radiation exposure used to be and currently still is the most crucial factor in protecting LEO microsatellites, increasingly the risk of debris collisions is becoming more important and will become the most important in the following 50 to 70 years. The authors conclude that microsatellite designers need to move their focus more towards defence from debris impacts as these, even if not resulting in catastrophic failure of the satellite, they will impact the attitude of the satellite [9].

- 3.2. PSD Enabled Sun Sensor**
- 3.3. Mechanical Design and Analysis**
- 3.4. Photodiode Simulation and Signal Analysis**
- 3.5. IoT Communication Enhancement with LEO Satellites**

4. Methodology

4.1. Prototype Development

4.1.1. Lifecycle

This section provides an overview of the Prototype Development Lifecycle.

Conceptualization and Requirements Definition

- The prototype must have four photodiodes in an xy pattern with respective circuitry required to output 0-5 Volts that will be read by an Arduino based Data Acquisition System (DAQ). The circuit must be able to react to light intensity changes, however the change will be at low frequency (below 1Hz) as a satellite attitude is considered to change only gradually.
- While the prototype may not have a high accuracy, it is hoped that it will be enough to measure light position changes roughly, even if at a low accuracy of 10° or 20° but this will remain to be seen.
- The prototype within the scope of this paper will show the ability to detect the position of light at normal room conditions, therefore it does not need to withstand temperature changes or radiation that a final product would require if deployed in space.
- Interface requirements: the prototype electrical output needs to be compatible with the Arduino Analog to Digital Converter (ADC) input. Therefore, the signal shall not go below 0 Volts or exceed 5 volts.
- Size and weight are not of high importance, but the device must fit in the testing equipment, which is the Renewable Energy Demonstrator arch. Preferably a height not higher than 5cm.

Theoretical Design

The prototype will be composed of three parts: a stripboard containing the components for the amplification circuit, a 3D printed Photodiode enclosure which will allow placing

the photodiodes in the correct positions, as the photodiodes have the legs at a smaller distance than the stripboard, and need to be placed quite close to each other, with the third part being the Arduino based DAQ. The third part to the

Sun Sensor Geometry and Aperture Design was decided to be in a T shape, providing an x-y layout with two photodiodes in the x direction and two photodiodes in the y direction. Combined with an aperture design that covers one half of each diode, as represented in Figure 4.1. This configuration is similar to Ortega et al. in their paper attempting to miniaturize a two axis Sun Sensor[10].

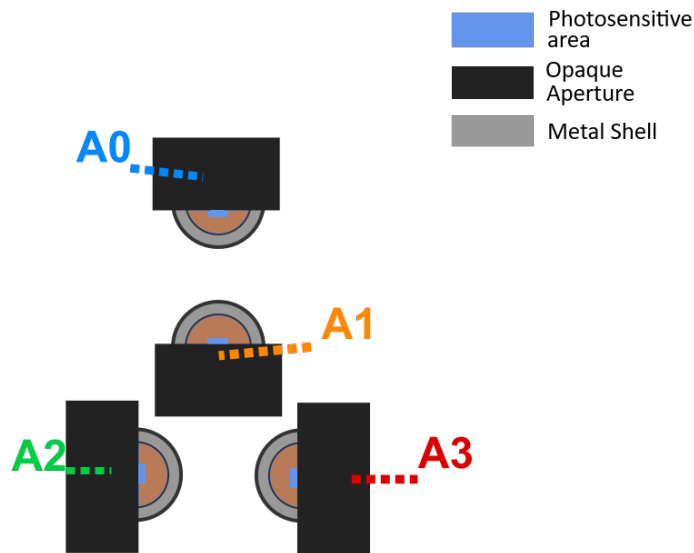


Figure 4.1.: Diagram of Photodiode Array with Apertures

Component Selection

The components chosen for the design of the prototype are detailed below. They were first placed on a BreadBoard and tests were performed to ensure the functionality of the circuit before moving them to a stripboard which would ensure the components are physically more stable and reduce the chance of faulty connectoins. Therefore, the same components were used for both BreadBoard and StripBoard prototyping. The circuit design and testing is gone into more detail in Section 4.1.2.

Photodiodes were researched and several options were found, most of which were quite expensive, such as 2D PSD type sensors like the Hamamatsu S5990 but were both prohibitivly expensive and Surface Mount Device style (SMD), which would have been harder

Table 4.1.: Electrical Components Used in Amplification Circuit

Component Type	Comp. Part Name	Component Value	Amount
Op-Amp	TI LM324-N	—	2
Photodiode	Hamamatsu S5971	—	4
Resistor	—	1 MΩ	4
Resistor	—	150 kΩ	4
Resistor	—	10 kΩ	4
Capacitor	—	1 μF	4
Stripboard	Veroboard	—	1
Screw terminal block	—	2-input	3

Table 4.2.: Components Used for DAQ System

Component Type	Component Part Name	Component Value	Amount
Microcontroller	Arduino Uno	—	1
Cable	USB cable	—	1
Computer	Laptop/Python	—	1

to prototype but would allow for much higher resolutions, while also complicating the project due to the more complex nature of PSDs. A decision was made to base the project on 1D photodiodes, and four Hamamatsu S5971 were purchased, which offered a good compromise in price and specifications: for under £10 a piece, the S5971 has the following specifications:

Table 4.3.: S5971 Photodiode Specifications

Parameter	Value
Spectral response range (λ)	320 to 1060 nm
Peak sensitivity wavelength (λ_p)	920 nm
Photosensitivity S (A/W) at λ_p	0.64
Photosensitivity S (A/W) at 780 nm	0.55
Photosensitivity S (A/W) at 830 nm	0.6
Short circuit current I_{sc}	1.0 μA
Dark current I_d (Typical)	0.07 nA ^{*3}
Dark current I_d (Maximum)	1 nA ^{*3}
Cutoff frequency f_c	0.1 GHz ^{*3}
Terminal capacitance C_t ($f=1$ MHz)	3 pF ^{*3}
Noise equivalent power NEP ($V_R=10$ V, $\lambda=\lambda_p$)	7.4×10^{-15} W/Hz ^{1/2}

$$V_R = 10 \text{ V}$$

Although the higher versions such as S5972-3 have better specifications, such as frequency cutoff of 1GHz and lower Dark current, these were not needed for our project, higher frequency cut off not needed due the static nature of the light source and dark current, while it could affect a case where one of the diodes is fully in the dark, a voltage

offset would be noticeable, but with a voltage resolution restricted by the Arduino DAQ to 4.88mV/step, it was deemed acceptable:

$$\begin{aligned}
 V_{\text{offset-TIA}} &= I_d \times R_f \\
 &= 0.07 \text{ nA} \times 1 \text{ M}\Omega \\
 &= 70 \mu\text{V}
 \end{aligned} \tag{1}$$

$$\begin{aligned}
 V_{\text{offset-total}} &= V_{\text{offset-TIA}} \times \text{Gain}_{\text{post-amp}} \\
 &= 70 \mu\text{V} \times 16 \\
 &= 1.12 \text{ mV}
 \end{aligned} \tag{2}$$

Equation 2 above shows the final dark current would be a maximum of 1.12mV which is below what the ADC can detect.

Operational Amplifier (OpAmp) choice was once again not a complicated choice due to the same arguments mentioned above re. photodiode selection: low frequency signal and reduced DAQ resolution. The LM324-N is a low-cost OpAmp which provides acceptable performance. The advantages in choosing this OpAmp is its ability to function

Table 4.4.: Operational Amplifier Specifications

Parameter	Value
DC Voltage Gain	100 dB
Unity Gain Bandwidth	1 MHz
Supply Voltage Range (Single)	3 V to 32 V
Supply Voltage Range (Dual)	± 1.5 V to ± 16 V
Supply Current	$700 \mu\text{A}$
Input Bias Current	45 nA
Input Offset Voltage	2 mV
Input Offset Current	5 nA
Input Common-Mode Voltage Range	Includes Ground
Differential Input Voltage Range	Equal to Supply Voltage
Output Voltage Swing	0 V to $V^+ - 1.5$ V

Internally frequency compensated for unity gain

Temperature compensated

on a single pole Power Supply, it is rather cheap while still offering 1MHz Unity Gain Bandwidth and is recommended for DC Gain which the type of signal our project aims to amplify. For example, the slew-rate characteristic is not mentioned on the datasheet because it is aimed at low frequency operation.

BreadBoard Testing

Once the circuit design was completed as seen in Figure 4.4, the components were placed on a BreadBoard to test the real circuit, as seen in Figure 4.2. There were several iterations, at first with only the Transimpedance Amplifier (TIA) and one photodiode- a design that when tested, resulted in a low Voltage output when testing with only the Light Emiting Diode (LED) light from the Renewable Energy Demonstrator (RED) testbench. This is due to the low light power of LEDs. A decision was made to add a secondary amplification circuit which raised the Voltage to a maximum 5V as designed. Further details on design in Section 4.1.2. The final BreadBoard design can be found in Figure 4.2.

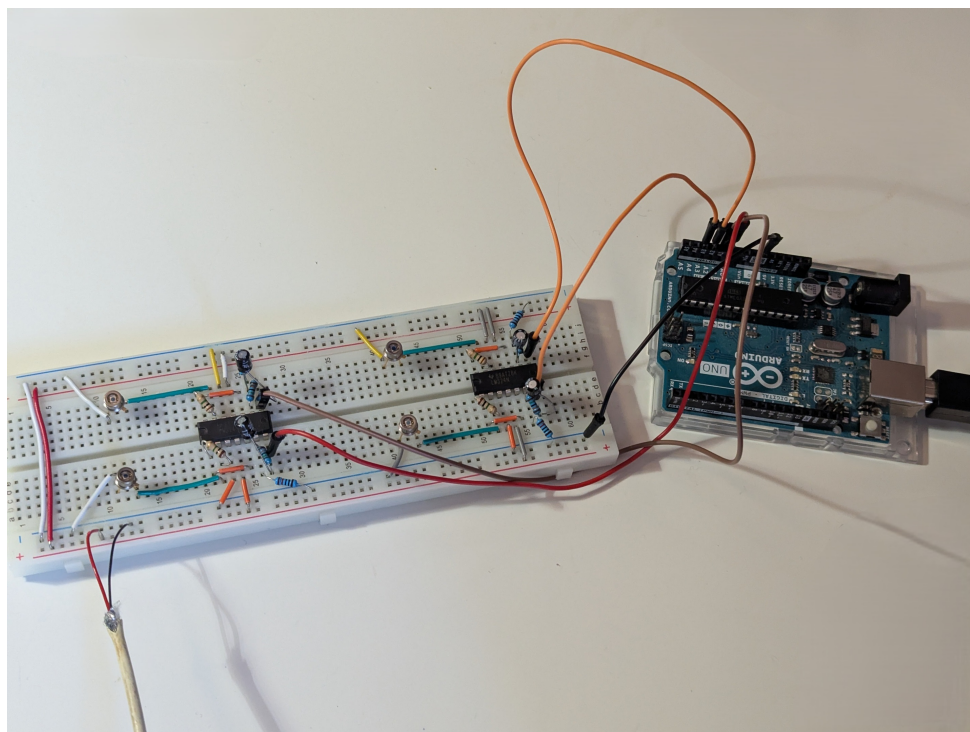


Figure 4.2.: Photo Of BreadBoard Prototype

Design Refinement

The major redesign was to add a second amplification circuit for signal conditioning to allow reading with the Arduino ADC making full use of the 5V range, as the Arduino ADC is a 10 bit ADC, making full use of the $2^{10} = 1024$ steps, otherwise the readings would be from 0 V to about 300 mV, with a much lower resolution between steps - the DAQ would be using a resolution of only $1024/16 = 64$ steps.

- Analyze test results
- Modify aperture design if needed

- Optimize photodiode configuration
- Update signal processing algorithms
- Refine PCB layout
- Improve firmware algorithms

Stripboard Prototype Development

- Implementing design improvements was easy on a BreadBoard
- Fabricate improved aperture
- Enhance housing design

BreadBoard Testing

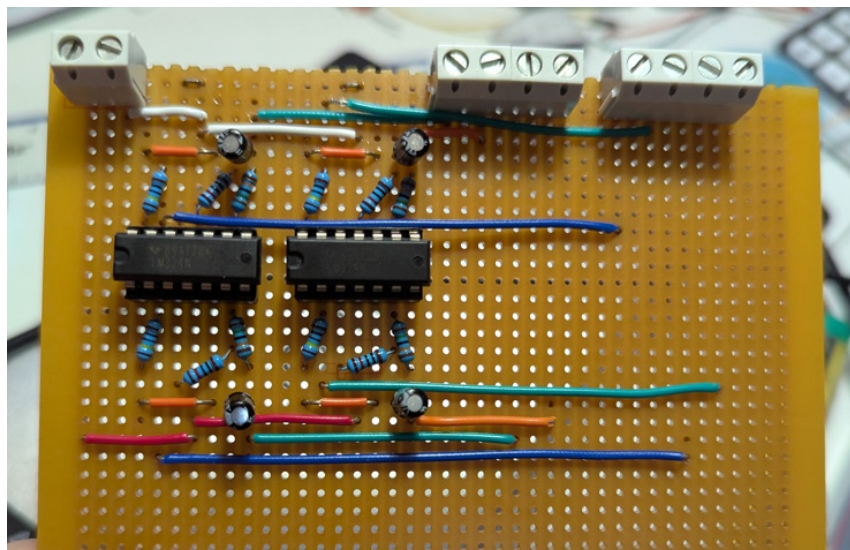


Figure 4.3.: Photo Of Stripboard Prototype

Comprehensive Testing

- Laboratory performance testing (angular accuracy, resolution)
- Improve Aperture
- Interface compatibility testing

Validation and Calibration

- Calibration procedure: match readings to simulation
- Create calibration fixtures
- Validate sensor performance against requirements

4.1.2. Signal Conditioning Circuitry

Photodiodes produce a certain amount of current when light hits the depletion region. Therefore, a larger depletion region is desirable, to capture more light and in turn produce more current. For this purpose the photodiode in our circuit is reverse-biased as can be seen in Figure 4.4 [11, p.155].

Transimpedance Amplifier (TIA)

A reverse-biased photodiode allows a current to flow from the cathode to anode which is connected to ground. This current is converted to a Voltage using a TIA with the following relationship:

$$V_{\text{out}} = -I_{\text{ph}} \cdot R_f \quad (3)$$

$$I_{\text{ph}} = P \cdot R_{\lambda} \quad (4)$$

Where P is Light Power (W) and R_{λ} is Responsivity (A/W).

$$V_{\text{out}} = -(P \cdot 0.5 \text{ A/W}) \cdot 1 \text{ M}\Omega \quad (5)$$

The TIA circuit makes use of an OpAmp as seen in Figure 4.4 that provides very high input impedance ($1G\Omega$) and allows the amplification of the signal without disturbing the photodiode current, therefore not affecting the readings. The inverting input is used in this configuration, which converts the negative current flowing from the cathode to the anode of the photodiode, into a positive voltage.

Secondary Amplification

Testing showed that even using a $1M\Omega$ resistor, the output voltage was too low (around 310mV) at our RED testbench' LEDs maximum brightness, as explained in Section 4.1.1.

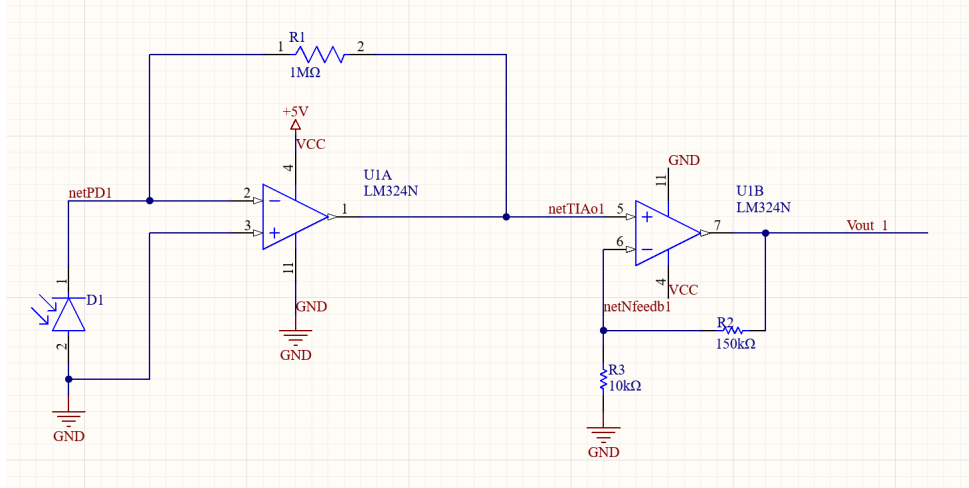


Figure 4.4.: TIA and Post Amplification Circuit in Altium Designer

To raise the maximum Voltage to the desired maximum of the ADC of 5V, a higher feedback resistor could be used, however this would introduce noise and would require more complicated TIA with feedback capacitors. Due to the LM324-N having 4 OpAmps, the decision was taken to implement a Secondary Amplification circuit. The non-inverting OpAmp configuration was chosen to maintain the voltage positive, which also means there is no need for a dual power supply and keeps the Voltage positive for the Arduino ADC. A simple calculation was made to figure out the required Gain of the circuit:

$$A = \frac{\text{required Voltage}}{\text{measured}} = \frac{5 \text{ V}}{0.31 \text{ V}} = 16.1 \quad (6)$$

Knowing the gain required, the feedback resistor was calculated by choosing a $10\text{k}\Omega R_f$ and rearranging the gain equation:

$$\begin{aligned} A &= 1 + \frac{R_f}{R_1} \\ 16 &= 1 + \frac{R_f}{10 \text{ k}\Omega} \\ 16 - 1 &= \frac{R_f}{10 \text{ k}\Omega} \\ 15 &= \frac{R_f}{10 \text{ k}\Omega} \\ R_f &= 15 \times 10 \text{ k}\Omega \\ R_f &= 150 \text{ k}\Omega \end{aligned} \quad (7)$$

This provides a gain $A = 16$ which is very close to the Gain required in Equation 6. Once the design was tested on a BreadBoard, it was transferred to a stripboard as pictured

in Figure 4.3.

4.1.3. Enclosure Design 3D print

This section provides an overview on the design and fabrication of the enclosure for the prototype. The enclosure is a critical component that houses the electronic components and provides protection against environmental factors. The design process involves several steps, including conceptualization, modeling, and fabrication.

Conceptualization

Material Selection

Fabrication Process

Testing and Validation

Iterations and Improvements

Final Enclosure Specifications and Documentation

4.2. Data Acquisition System

4.2.1. Functional Requirements

The output signal from the photodiode array amplifier is required to be converted to digital form for post-processing. This requirement is filled by designing a Digital Acquisition System (DAQ) capable of recording the signal from the four photodiode circuits simultaneously. The choice of design was conceived by analyzing the analog signal and determining some basic requirements of the Analog to Digital Converter (ADC) the DAQ must possess.

Analog Signal Characteristics

- The signal is four channel, one per photodiode, and between 0 and 5 Volts, as the TIA and post amplification was designed specifically for this output.
- Close to DC frequency, i.e., static in nature, due to light intensity remaining static under most tests. One test is performed at 0.2Hz, which is still very low frequency, with the light completing a semicircular arc once in 130 seconds (26 positions of 5 seconds each).
- Later in testing it was found that the signal is impacted by interference of 400mVpp at a frequency fluctuating from 160kHz to 180kHz from the RED testbench power supply, as pictured in Figure 4.5.

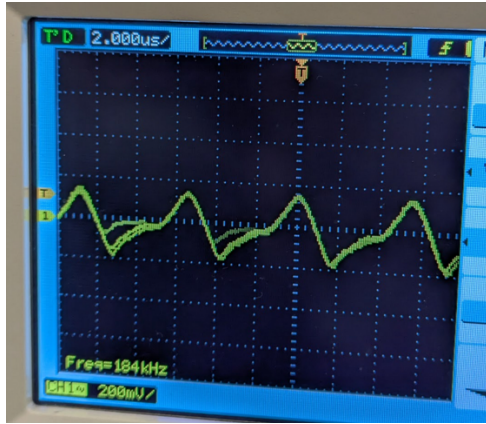


Figure 4.5.: Signal Noise Analysis, oscilloscope AC coupled

CSV Data Structure and Format Specification is as follows:

The output of the DAQ is to be saved in Comma Separated Values (CSV) file format, with columns as follows: Sample(nr.), Time(ms), A0(V), A1(V), A2(V), A3(V). This allows for easy post-processing and plotting.

4.2.2. Design Approach

The characteristics of the signal being low frequency, combined with the requirement to read all four signals simultaneously and in sync, meant two things: the Sampling Rate could be quite low due to Nyquist theorem telling us that the sampling rate must be at least twice the frequency of the signal being sampled, in order to maintain the original signal without aliasing [1, p. 146]. Therefore a low performing ADC is acceptable for a signal changing at under 1Hz. And secondly, the DAQ must support sampling from at least four analog inputs. These requirements meant that a cheap Arduino based DAQ could fit perfectly the needs of the project: it is powered by the Atmega328P which has an included ADC of 15 ksps [12, p.205]. And the Arduino Nano has four analog inputs.

Arduino Programming

The Arduino-based DAQ will require both a C++ program written for the Arduino itself, as well as a program or script on the PC receiving the digitized signal, this is because the Arduino lacks both the memory requirements and capability to store the recorded digitized signal to some internal memory.

The Arduino C++ Program must be able to listen to commands from the user on the PC receiving, start a recording, and immediately transmit to the PC over serial communication.

4.2.3. Technical Specifications

Arduino Code

The Arduino Code which uses the Arduino ADC is formed of the setup() function triggered once at the start/reset of the device and a standard continuous loop triggered after setup completes. Inside the loop, two if statements check for instructions from the PC script. The recording time limit is hardcoded as a global function. Figure 4.6 shows the algorithm as a Flowchart that checks for Serial data in, waits for a command to start recording, and if recording time has reached the preset limit, it stops recording, sends the last values to the Python script on the PC and a "recording_stopped" command. A FSM diagram is also available in Figure 4.7. The pseudocode used while designing the Arduino side of the DAQ system, is available in Listing 4.1. The final code is available in Appendix A.1.1.

The Atmega328P does not have a separate ADC clock input, therefore the CPU clock is used by first dividing by a default rate of 128, this divider is changed to 16 by changing bits 2-0 to 100, as per [12, p.219]. This increases the clock speed available to the ADC for a higher sampling rate. This results in a 1MHz clock signal to the ADC (16MHz/16) which seemed needed when dealing with multiplexing four analog inputs to a single ADC. The process is as follows:

Original ADC Clock Speed (with default prescaler of 128):

$$f_{\text{ADC-default}} = \frac{f_{\text{CPU}}}{\text{Prescaler}_{\text{default}}} = \frac{16 \text{ MHz}}{128} = 125 \text{ kHz} \quad (8)$$

Optimized ADC Clock Speed (with modified prescaler of 16):

$$f_{\text{ADC-optimized}} = \frac{f_{\text{CPU}}}{\text{Prescaler}_{\text{optimized}}} = \frac{16 \text{ MHz}}{16} = 1 \text{ MHz} \quad (9)$$

Conversion Time Calculations: ADC requires approximately 13 clock cycles for each conversion [12, p.208] Optimized ADC Clock Speed (with modified prescaler of 16):

$$T_{\text{conversion-default}} = 13 \times \frac{1}{f_{\text{ADC-default}}} = 13 \times \frac{1}{125 \text{ kHz}} \approx 104 \mu\text{s} \quad (10)$$

$$T_{\text{conversion-optimized}} = 13 \times \frac{1}{f_{\text{ADC-optimized}}} = 13 \times \frac{1}{1 \text{ MHz}} \approx 13 \mu\text{s} \quad (11)$$

Time required to sample all 4 analog inputs:

$$T_{\text{4channels-default}} = 4 \times T_{\text{conversion-default}} = 4 \times 104 \mu\text{s} \approx 416 \mu\text{s} \quad (12)$$

$$T_{\text{4channels-optimized}} = 4 \times T_{\text{conversion-optimized}} = 4 \times 13 \mu\text{s} \approx 52 \mu\text{s} \quad (13)$$

Maximum theoretical sampling frequency for all 4 channels:

$$f_{\text{sampling-max-default}} = \frac{1}{T_{\text{4channels-default}}} = \frac{1}{416 \mu\text{s}} \approx 2.4 \text{ kHz} \quad (14)$$

$$f_{\text{sampling-max-optimized}} = \frac{1}{T_{\text{4channels-optimized}}} = \frac{1}{52 \mu\text{s}} \approx 19.2 \text{ kHz} \quad (15)$$

Actual limited sampling frequency (based on minSampleInterval = 2ms):

$$f_{\text{sampling-actual}} = \frac{1}{2 \text{ ms}} = 500 \text{ Hz per channel} \quad (16)$$

Effective data rate across all channels:

$$\text{Data Rate} = 4 \text{ channels} \times 500 \text{ Hz} = 2000 \text{ samples/second} \quad (17)$$

In real testing the actual sampling rate was closer to 330Hz for 5 second recordings or 100Hz for a 2 minute recording - after some investigation the only explanation was the relatively small size of the transmission buffer implemented by the Serial C++ library. The buffer is of only 64 bytes, and when it fills, the function Serial.write() (used by println()) will block the write until there is space in the buffer[ref:arduino.cc/serial.write]. As our line of text is quite long "498,5000,0.059,0.054,0.073" for example has 26 characters (last line of a 5 second recording). For larger recording length, where the first and second column, Sample and Time, can get quite large, the sampling rate decreased considerably, but was kept constant (around 10ms for a 2 minute recording). Presumably due to optimization in the Arduino Serial Hardware/Software or compiler, it remains constant at 10ms. However this was not investigated further as for our near-DC signal, even 10ms

was a fast enough sampling rate for our DC-like signal.

```
1 recordingDuration = 5000 // for how long to record in milliseconds
2
3 minSampleInterval = 2      // control how fast to sample to avoid
4                           // relying on Arduino performance
5 // Initialize serial communication
6 // Initialize analog inputs
7 // Setup ADC
8
9 // Infrom PC listening on Serial Connection: Arduino is ready to
10 record
11 Serial.print("Arduino_DAQ_Ready")
12 // enter the loop
13 void loop(){
14     //listen for command from PC script:
15     String command = Serial.read()
16     //set system state
17     if (command == "START"){
18         // Send header of csv
19         Serial.println("Sample,Time(ms),A0(V),A1(V),A2(V),A3(V)")
20         // keep track of system state
21         state = recording
22         // keep time
23         startTime = currentTime()
24         // send confirmation
25         Serial.println("recording in progress")
26     }
27     // check if recording
28     if (state == recording){
29         // check if within recording period
30         currentTime = currentTime()
31         elapsedTime = currentTime - startTime
32         if(currentTime <= recordingDuration){
33             // Also check not recording too fast
34             if(currentTime - lastSampleTime >= minSampleInterval){
35                 sampleCount++;
36                 // Start each row with sample count and time of sample
37                 String currentCSVrow = String(sampleCount) , string(
38                 elapsedTime)
39                 // Multiplex through all analog inputs
40                 for (int = 0;i<4;i++){
41                     //read raw values
42                     rawValue = analogRead(analogInputs[i]);
43                     // compute real value
44                     voltage = rawValue * 5/1023
45                     // add value to current row to send
46                     currentCSVrow += String(voltage)
```

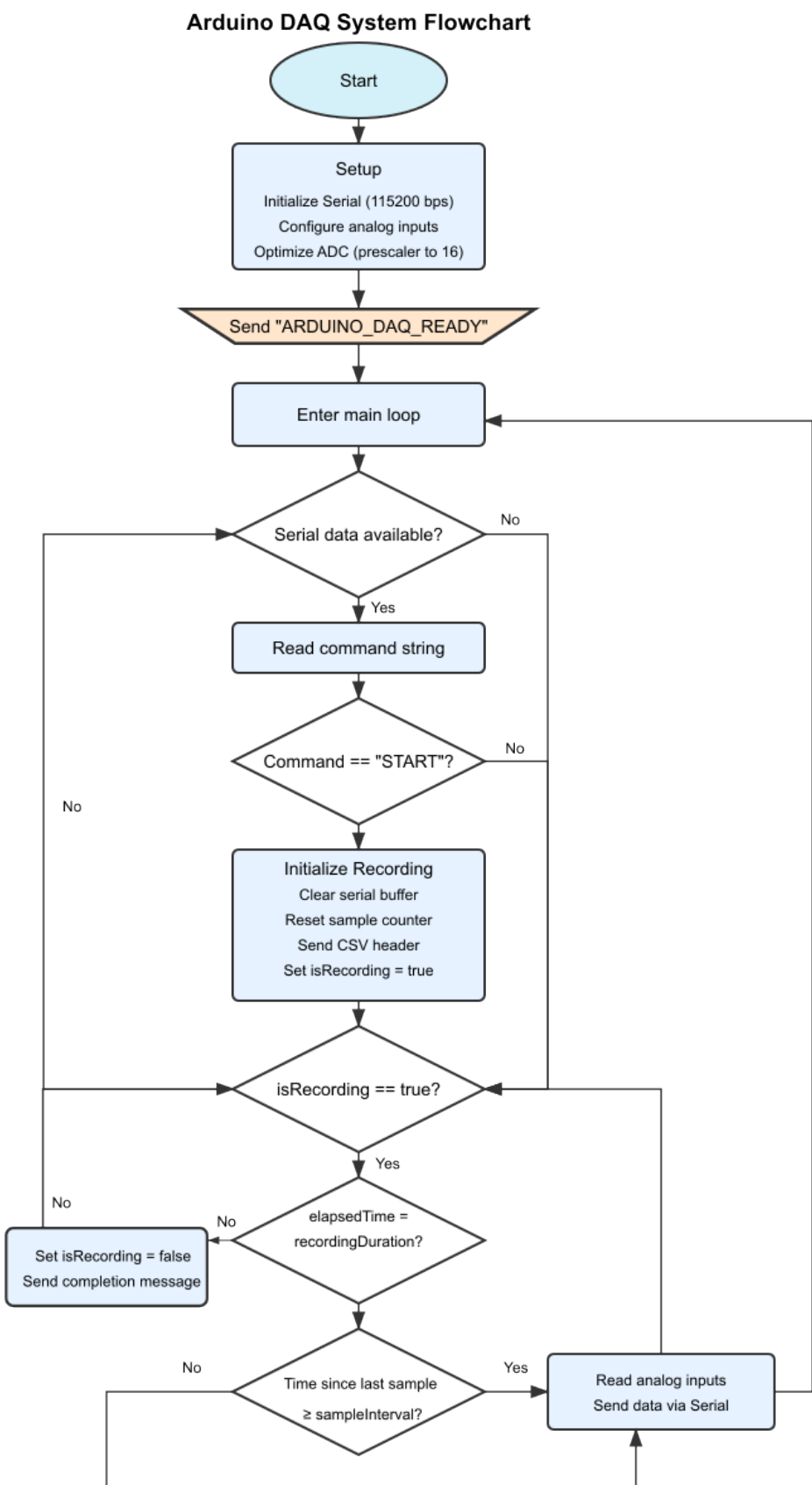


Figure 4.6.: Flowchart Arduino DAQ C++ program

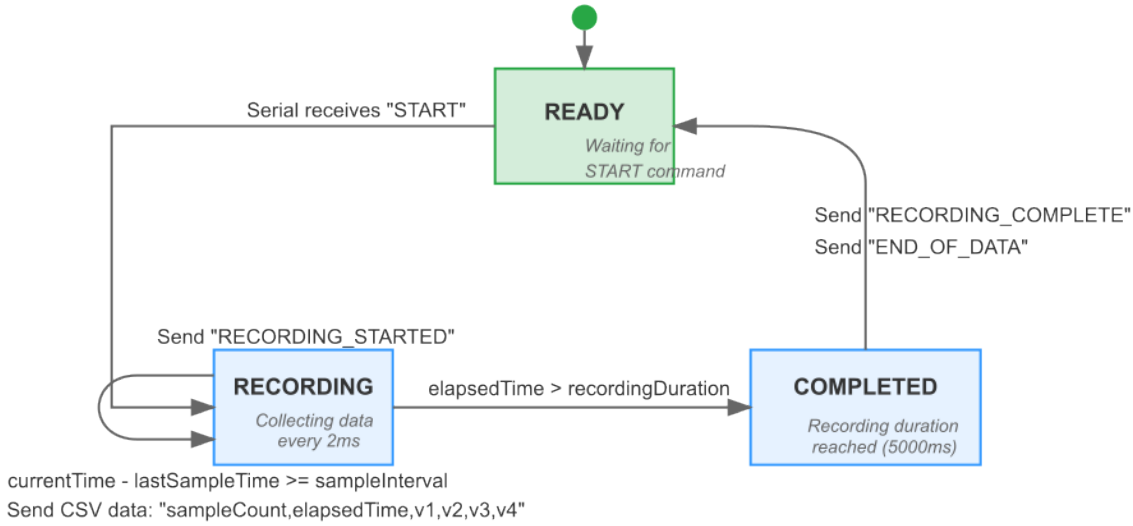


Figure 4.7.: FSM Arduino C++ LOOP

```

45
46     }
47     // Send completed row to PC
48     Serial.println(currentCSVrow)
49 }
50 }
51 // end recording
52 else{
53     state = notRecording
54     // tell PC recording finished
55     Serial.println("Recording_finished")
56 }
57 }

```

Listing 4.1: Arduino DAQ PseudoCode

Sampling Rate Details Several factors restrict the sampling rate:

Sample Interval Setting The most direct limitation is the `sampleInterval` constant set to 2ms in the code. It was meant to avoid having random sampling rates based on the number of computations required. This means samples are taken no more frequently than every 2 milliseconds (500 Hz theoretical maximum) of all four channels. The "jump" to sample the next channel is not limited in the code, but it will take 13 clock cycles, (ie. around 13 μ s at 1MHz ADC clock) to switch to the next channel.

ADC Prescaler Configuration The ADC prescaler is set to 16 (from the default of 128) with this line:

```
ADCSRA = (ADCSRA & 0xF8) | 0x04;
```

This increases the ADC clock to $16\text{MHz}/16 = 1\text{MHz}$. With each conversion taking 13 ADC clock cycles, the theoretical maximum sampling rate is about 76.9kHz for a single channel.

Serial Transmission Overhead Each sample requires formatting and sending data over serial:

```
String dataString = String(sampleCount) + "," + String(elapsedTime);  
// ... format and add voltage values ...  
Serial.println(dataString);
```

This string creation and serial transmission takes some time to process as mentioned earlier.

Serial Baud Rate The code uses 115200 bps, which limits how quickly data can be transmitted. Each sample in this format might be around 30-40 bytes, which means ~3000-3800 samples/second theoretical maximum throughput.

String Operations The use of the Arduino `String` class is memory-intensive and can cause fragmentation over time, potentially causing the slowdowns noticed during testing with larger timeframes (and longer strings).

Python Script

The digitized signal must be interpreted and saved on the PC. This is done via a python script which listens to the Serial port from the arduino. The signal then also required cleaning from RF interference discovered during testing. In Figure 4.8 a flowchart is produced showing the way the script works: after initial setup that sets up the Serial Communication, the script waits for a "DAQ_READY" signal from the Arduino. Once this is received, a csv file is created and the script sends a "START" signal which the Arduino interprets and starts sampling and sending the data. The script receives each line and saves it in the new CSV, and continues to record data until the Arduino sends a "RECORDING_COMPLETE" signal - which will happen when the recordingDuration is reached. At this point the python script performs the following post-processing steps:

The `filter_and_save_data()` function's purpose is mainly to correctly interpret the CSV. It takes a csv with the raw voltage values, saves them into a Pandas DataFrame for easier manipulation and sends each channel to the `apply_lowpass_filter()` function which will be described below. `filter_and_save_data()` pseudocode is produced in Listing 4.2.

```

1  FUNCTION filter_and_save_data(filename)
2      // Load data from CSV file into a table structure
3      data_table = READ_CSV(filename)
4
5      // Streamline the data by converting text to numbers
6      FOR EACH column IN data_table
7          CONVERT column values to numeric type
8          IF conversion fails for any value
9              REPLACE with NaN (Not a Number)
10     END FOR
11
12     // Remove any rows containing NaN values
13     REMOVE all rows with NaN values from data_table
14
15     // Calculate sampling frequency
16     time_differences = CALCULATE differences between consecutive time
17     values
18     typical_time_difference = FIND median of time_differences
19     sampling_frequency = 1000.0 / typical_time_difference // Convert ms
20     to Hz
21
22     // Process each data channel
23     channel_list = ["A0(V)", "A1(V)", "A2(V)", "A3(V)"]
24
25     FOR EACH channel_name IN channel_list
26         IF channel_name EXISTS in data_table
27             filtered_values = APPLY_LOWPASS_FILTER(original_values,
28             sampling_frequency)
29             ADD new column named channel_name + "_filtered" with
30             filtered_values
31         END IF
32     END FOR
33
34     // Save results to new file
35     new_filename = REMOVE_EXTENSION(filename) + "_filtered.csv"
36     WRITE data_table TO new_filename
37
38     RETURN new_filename
39 END FUNCTION

```

Listing 4.2: Python `filter_and_save_data()` PseudoCode

Python DAQ Script Flowchart

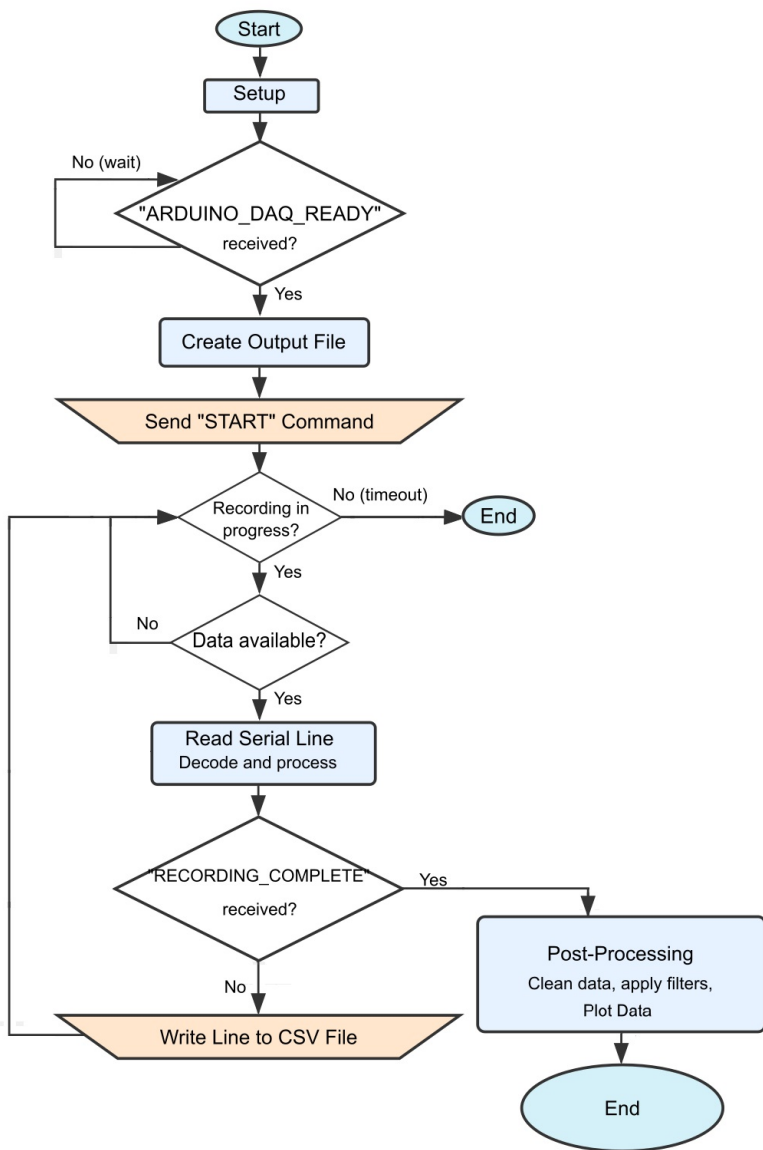


Figure 4.8.: Python Script Flowchart

The apply_lowpass_filter() function was created and integrated into the script once it was observed that the RED testbench used was introducing noise as seen in Figure 4.5. The benefit of using an already built testbench that could place the light at exact positions repeatedly, meant it would make sense to accept the noise and just filter the data, as the signal of interest was very low frequency while the noise was around 170kHz. The filter could be relatively simple, due to the large frequency difference between noise and signal. A 4th order Butterworth IIR filter was deemed acceptable and a low cut-off frequency of 1Hz or 2Hz was used for the static readings. This was found to be acceptable for the test involving light location at a frequency of 0.2Hz the transition of the light from one position to another was still visibly sharp. The post-processing is not the only reason light transition would not appear instantaneous on the Voltage graph, another reason is the amplification circuit which has a 1Hz cutoff frequency via the feedback capacitor on the secondary-amplification OpAmp circuit. The pseudocode of the function that creates the low-pass digital filter and filters the data is reproduced in Listing 4.3. The butter() function from the library signal is used, from the scipy package [13] which is a free and open source library offered to the scientific community. Before feeding the cutoff frequency to the filter, it is normalized to the Nyquist rate, which means it is between 0 (DC) and 1 (Nyquist frequency), and therefore the filter can be applied no matter the sampling rate. As Schafer and Oppenheim explain in "Discrete-Time Signal Processing" Third Edition: "The frequency scaling or normalization in the transformation from $X_s(j\Omega)$ to $X(e^{j\omega})$ is directly a result of the time normalization in the transformation from $x_s(t)$ to $x[n]$ " [1, p.171]. When creating a digital filter, this normalization becomes crucial because in the continuous-time domain, frequencies are measured in Herz and in the discrete-time domain, frequencies become relative to the sampling rate. The relationship between these two frequency domains is given by $\omega = \Omega T$, where:

- ω is the normalized digital frequency (radians/sample)
- Ω is the analog frequency (radians/second)
- T is the sampling period (seconds)

However, when implementing IIR filters like the Butterworth filter used for our purpose, the bilinear transformation is employed to convert from the continuous-time domain to the discrete-time domain. This transformation introduces frequency warping, where the relationship between the analog and digital frequencies becomes:

$$\omega = 2 \arctan(\Omega T_d / 2)$$

where T_d is the sampling period. This nonlinear relationship compresses the infinite analog frequency range $(-\infty, \infty)$ into the finite digital frequency range $(-\pi, \pi)$. The

warping effect is more pronounced at higher frequencies, meaning that in our case it would not be noticeable [1, p.529-530].

A critical property of the bilinear transformation is stability preservation. In the analog domain, a stable system has all poles in the left half of the s-plane reproduced in Figure 4.9. The bilinear transformation maps the entire left half of the s-plane to the interior of the unit circle in the z-plane. This ensures that the 4-pole Butterworth filter, which is stable in the continuous-time domain, remains stable when converted to its discrete-time equivalent.

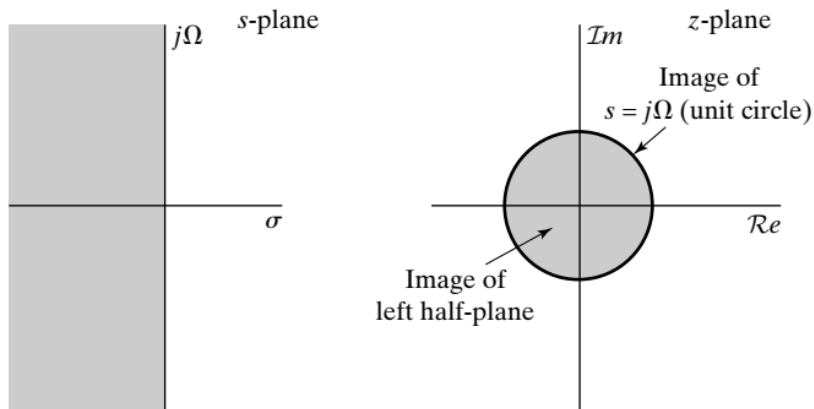


Figure 4.9.: Mapping of the s -plane onto the z -plane using the bilinear transformation [1, p.130]

The filter Frequency Response was reproduced in Figure 4.10 using the `scipy.signal.freqz()` method. The actual implementation uses `filtfilt()` which applies the filter twice, effectively doubling the filter order [14]. This affects the transition steepness and phase response. The Discrete-Time Transfer Function is reproduced in Equation 18.

$$H(e^{j\omega}) = \frac{b[0] + b[1]e^{-j\omega} + b[2]e^{-j2\omega} + b[3]e^{-j3\omega} + b[4]e^{-j4\omega}}{a[0] + a[1]e^{-j\omega} + a[2]e^{-j2\omega} + a[3]e^{-j3\omega} + a[4]e^{-j4\omega}} \quad (18)$$

```

1  from scipy import signal
2  FUNCTION apply_lowpass_filter(data, sampling_rate)
3      // set hardcoded filter values
4      cutoff_freq = 2;
5      filter_order = 4;
6      // calculate Nyquist Frequency and Normalized cut_off
7      nyquist = 0.5 * sampling_rate;
8      norm_cutoff = cutoff_freq / nyquist;
9      // generate numerator b and denominator a polynomials
10     b, a = signal.butter(filter_order, norm_cutoff, filterType = LOW);
11     // filter the data
12     filtered_data = filter(b,a,data);

```

```

13
14     return filtered_data;

```

Listing 4.3: Python apply_lowpass_filter() PseudoCode

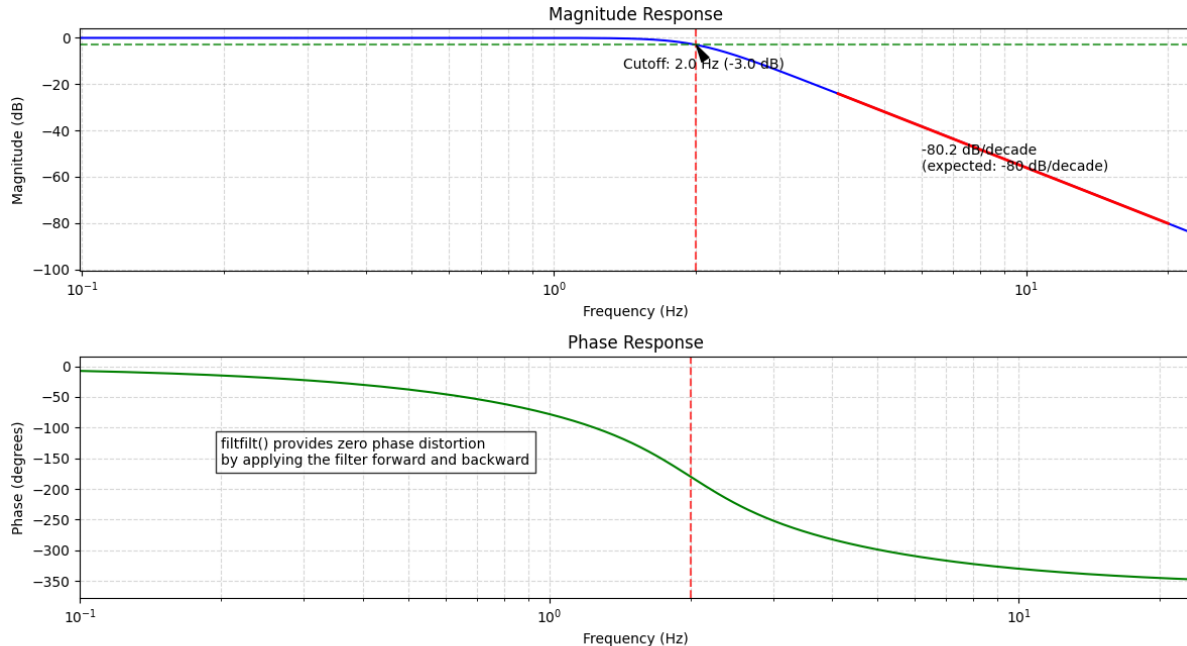


Figure 4.10.: Frequency Response of 4-pole Butterworth Low-Pass Filter (Cutoff: 2.0 Hz, Order: 4, Fs: 500 Hz)

4.2.4. Testing Strategy

The testing was done incrementally with each new version of the program, many tests were carried out as the development was dependent on both C++ code on the Arduino and the Python script on the PC to somewhat work together. At first the C++ program was tested by listening to the output in the Serial Monitor of the Arduino IDE and sending commands the same way. Debug Serial.println() lines were used to ensure the loop on the Arduino was in the correct state. Once the C++ program seemed to somewhat work as intended, the Python script was implemented to send / receive.

4.2.5. Evaluation of design

The design was tested iteratively while making changes to the code with a signal generator at first to simulate a steady known input signal and compare readings on the Arduino IDE Serial Monitor. Once the Python script was fully working, tests were performed again for

the python script's ability to read the values sent correctly. An issue was identified where sometimes the Arduino would send the column headers not at the beginning of the CSV and these lines had to be cleaned manually. This could be due to Serial buffer issues but was not investigated. Later an attempt was made to perform the cleaning programatically by creating a function in the script to do so.

4.3. Renewable Energy Demonstrator Testbench

For testing the capability of the Sun Sensor to correctly detect the location of the light source, a test bench was required that could reliably place the location of the light at a precise location repeatedly. For this purpose we used a project built by our colleagues in the European Project Semester year 2021/22 who created just such a device intended for demonstrating renewable energy creation live [15]. Their device was able to demonstrate the energy levels created by a Photovoltaic (PV) cell by light emitted at different angles. The light emission would change location based on time of day and the PV cell readings would show the difference in energy. Further the PV cell was controllable by a joystick to point the PV Cell at the optimum angle for the highest energy capture. For our project, the arch and LED strip were used for outputting light from different angles.

Analysis of High Frequency Noise in AC-DC Power Supply

Interference structure of around 170kHz with 400mV peak-to-peak was detected on the signal being received while the RED testbench was on as shown in Figure 4.5. This noise could be generated by several factors in the AC power supply used by the RED testbench:

1. **Switching frequency harmonics** — If it's a switch-mode power supply (SMPS), the fundamental switching frequency or its harmonics might be causing the noise. Many SMPS operate in the 50–200,kHz range.
2. **Poor filtering** — Inadequate output filtering (insufficient capacitance or poor quality capacitors) can allow switching noise to appear on the output.
3. **Improper design of magnetics** — Issues with the transformer or inductor design could cause ringing or oscillations.
4. **Resonance in the circuit** — Parasitic capacitance and inductance forming a resonant circuit at around 170,kHz.
5. **Control loop instability** — PWM controller instability can cause oscillations.
6. **Ground loops or poor PCB layout** — Improper grounding or PCB layout can create noise paths. [16]

To avoid spending time diagnosing and trying to repair the testbench, an easier solution was reached: performing digital filtering of the acquired signal in post processing. Due to the signal of interest being close to DC - frequencies much lower than 1Hz, and the noise being high frequency, around 175kHz, a simple digital Butterworth filter with a cutoff frequency at around 1-2 Herz was found to be a good solution.

The only remaining issue was that this noise would sometimes trigger the internal components of the testbench, unintentionally triggering the button press from the control interface that was changing the light position, but it happened so rare that it was not a major concern.

4.4. Software Model

4.4.1. Introduction

A Python model was constructed to provide a simulation of the movement and intersection of rays from a movable source to evaluate sensor performance and compare these results with practical experiments. The model allows for a number of configurable parameters:

- The trajectory of the light source 3D space, which moves in configurable discrete increments.
- The placement of any number of sensors and apertures, including their dimensions.
- The form of the output data, including as a static, or animated graphic.

Affording flexibility for the model to simulate any sensor topology under a variety of conditions.

4.4.2. Theory and Concept

The system is modelled in 3D space, consisting of planes and lines. Each line is defined by vectors representing position and normal direction, $\vec{A} = (a, b, c)$ and $\vec{u} = (\alpha, \beta, \gamma)$. The planes are defined by the vectors $\vec{P} = (l, m, n)$ and $\vec{n} = (\lambda, \mu, \nu)$, respectively.

Ray projection, from a source plane to a sensor plane, is modelled using the parametric equation of a 3D line (19). This allows each ray to be described in terms of a parameter t , which enables the calculation of the intersection points between the light rays and the sensor plane.

$$\frac{x-a}{\alpha} = \frac{y-b}{\beta} = \frac{z-c}{\gamma} (= t) \quad (19)$$

Where the intersection coordinates (x, y, z) occur within a target area, a hit occurs, representing illumination.

For any given combination of source plane, and sensor plane, the t parameter is calculated using the Line-Plane Intersection equation

$$t = \frac{\vec{n} \cdot \vec{P} - \vec{n} \cdot \vec{A}}{\vec{n} \cdot \vec{u}} \quad (20)$$

4.5. Material Analysis and Selection

4.5.1. Material Selection and Requirements

The PCB will be operated in harsh environmental obstacles from strict requirements in both space and weight. PCB must withstand the extremities of immense pressures and vacuums, polarising temperatures, vibrations, impacts, space radiation and more. Generally, the materials for PCB made for space conditions are either polyimide or ceramic, as they can withstand extremely harsh conditions [17]. Commonly materials used for space PCB include polyimide, PTFE and alumina [18].

4.5.2. External Factors

The PCB needs to sustain itself when it is launched into and deployed to outer space from the extreme heat it will experience from -200°C in the shadow of a celestial body to over 200°C when sunlight exposes on it

Extreme Temperature Variations

Space exposes PCBs to extreme temperature fluctuations, which can affect their structural integrity and performance. Materials must maintain their thermal stability and dimensional consistency across a wide temperature range.

The temperature in space varies dramatically, ranging from extreme cold in the shadow of celestial bodies to scorching heat under direct solar exposure [19]. Materials expand and contract, with the magnitude of the dimensional change determined by the material's Coefficient of Thermal Expansion (CTE) [20]. When different materials in a PCB assembly have differing CTEs, the repeated cycles of expansion and contraction can result in considerable mechanical stresses at their interconnections [19].

These stresses may result in severe failures such as solder joint cracking, PCB layer delamination, and even circuit malfunction [19]. As a result, materials with naturally low CTE values, such as ceramic PCBs, are widely used in space applications to reduce these concerns [19]. A material's capacity to resist multiple temperature cycles without degradation is also critical for long-term reliability in space missions [18].

Ionizing Radiation

High-energy radiation, including cosmic rays, solar particles, X-rays, and UV radiation, exists throughout the space environment [19].

This ionising radiation poses a significant risk to the performance and durability of electronic components, particularly those found on PCBs. Radiation exposure can impair semiconductor performance, potentially causing data corruption via bit flips and resulting in a steady loss of material properties with time [21].

Celestial sources and the sun emit ionizing radiation that can disrupt the PCB's functionality and degrade the semiconductors' performance, hence, to protect the sensitive electronic components from being damaged by radiation, the PCBs must be made from radiation-hardened materials.

To mitigate these negative effects, radiation-hardened materials are frequently used in space-grade PCBs. Ceramic substrates, for example, are more resistant to radiation than many biological materials. Specialised coatings are also used to give another layer of protection to delicate electrical components [21].

The use of materials with intrinsic radiation resistance is an important design concern for ensuring the ongoing operation of electronic devices in the harsh radiative environment of space [22].

4.5.3. Internal Factors

Mechanical Stresses

The PCB, housing and aperture will experience mechanical stresses during the launch and deployment in the spacecraft, from the vibrations generated from the launch and deployment phase it can cause structural damage. To mitigate this issue there are in place shock-absorbing mechanisms that include the PCB material being flexible and conformal coating to safeguard the electronic components' integrity. Flexible PCBs are more effective at absorbing disturbances and vibrations compared to rigid PCBs.

PCBs are subjected to immense mechanical strains throughout a space mission's launch and deployment phases. The tremendous vibrations and shocks produced during launch, along with the high gravitational forces experienced, can put great stress on every component of the PCB [19].

Furthermore, the deployment of solar arrays and other spacecraft features may cause additional mechanical stress [19]. These forces can cause structural damage to PCBs, such as board cracking, layer delamination, and the breakdown of solder junctions that connect components [19].

To address these issues, designers frequently use shock-absorbing mechanisms, such as flexible PCB materials like polyimide, which are more effective at absorbing vibrations than rigid counterparts. Conformal coatings are also used to give an extra layer of pro-

tection against physical damage during launch and deployment [19]. Furthermore, precise PCB layout design is required to guarantee a more even distribution of mechanical loads across the board [19].

Outgassing and Vacuum

Outgassing is another internal factor which is when manufacturing the PCB, outgassing is a soldering wave defect that traps air within a PCB. This is a major issue as it can lead to the PCB impairment from the cavities or blowholes created by the air inside. This is often a result of defective manufacturing and poor material selection choices.

There is a strict size and weight limit for the PCBs because of the tight space in the spacecraft, thus the PCB must be compact and lightweight whilst maintaining equilibrium that it does neither compromise on the functionality and the structure of the PCB.

The near-perfect vacuum of space poses an additional notable challenge for PCB materials. Materials in this environment can undergo outgassing, which is the release of trapped volatile chemicals [18]. These outgassed compounds can have harmful impacts on delicate spacecraft equipment [23]. Optical instruments, such as cameras and telescopes, are especially susceptible to contamination by outgassed materials, which can deposit on their surfaces and degrade performance [19]. Similarly, thermal control surfaces can be influenced, affecting their ability to regulate the spacecraft's temperature [20].

Furthermore, the release of gases near high-voltage components can raise the risk of corona discharge, which could hinder electronic operations and cause damage [20]. To address these difficulties, the materials used in space-grade PCBs must have low outgassing qualities. Polymers such as polyimide and PTFE (Teflon) are widely used because of their extremely low outgassing properties, which help to protect the integrity of sensitive spacecraft components and systems [19].

4.5.4. PCB Material Selection

High-T_g FR-4

While not as extensively used as polyimide or ceramics in the most extreme space environments, high-T_g FR-4 laminates find application in scenarios where thermal conditions are less severe, such as within crewed spacecraft like the International Space Station [18]. These epoxy-based laminates possess a higher glass transition temperature (T_g) compared to conventional FR-4, providing greater stability at elevated temperatures. Epoxy laminates typically have a glass transition temperature between 150-170°C [18].

Using GRANTA EduPack 2022 R2, we found that FR-4 variations with dissipation factors (DF) of 0.015, 0.02, and more than 0.02 would be excluded from our nanosatellite PCB application. These materials were eliminated because they have larger signal losses at communication frequencies, reducing power efficiency in our power-constrained

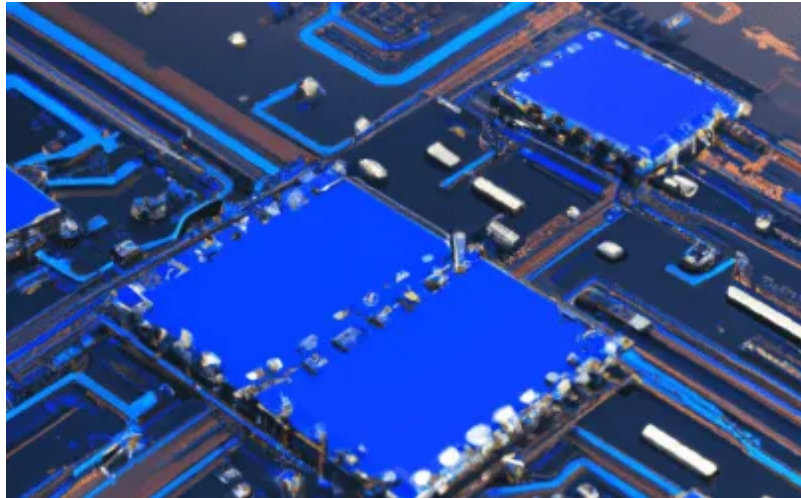


Figure 4.11.: FR-4 PCB [2]

nanosatellite design. The increased signal attenuation will compromise the reliability of data transmission and could also raise thermal loads on the board. Furthermore, ordinary FR-4 materials often have lower glass transition temperatures, which poses dimensional stability problems during the severe heat cycling encountered in the space environment (-60°C to +100°C). These restrictions would negatively impact both the electrical performance and long-term dependability of the PCB, making these materials unsuitable for the demanding circumstances of the space environment.

Even FR-4.0 with $DF < 0.01$, while superior to other FR-4 varieties, has limits for space applications. Its glass transition temperature range (130-180°C) has a lower limit that may not be adequate for intense orbital thermal cycling. Its thermal expansion coefficient and mild outgassing properties in vacuum may jeopardise long-term reliability and contaminate sensitive optical components. Although more expensive, more specialised space-grade materials would be preferable for maximum performance in nanosatellite applications.

Polyimide

Research is conducted about materials suited for space PCBs, a prominent material used is Polyimide (PI), the common "space age" material with the highest performing class out of plastics.

Polyimide is a flexible polymer that is commonly used as a substrate material in space-grade printed circuit boards due to its inherent flexibility and lightweight nature [18]. This flexibility enables polyimide-based PCBs to effectively absorb mechanical stresses encountered during the dynamic stages of launch and spacecraft deployment. Furthermore, polyimide has strong thermal stability, which allows it to survive temperature fluctuations in space to some extent [18]. It also has low outgassing qualities, which are critical for avoiding contamination of sensitive spacecraft components [19]. However,

Polyimide is generally regarded as less suited for applications involving high levels of radiation exposure than other materials such as ceramics [18]. For over three decades, DuPont's Pyralux laminates and Kapton polyimide films have been widely used in the aerospace and defence markets, with applications ranging from multi-layer insulation to wire wrapping and flexible circuit interconnects on solar panel backplanes [24]. The Mars Rover Pathfinder also pioneered the use of adhesiveless laminate in space, using Pyralux AP material [24].

A material analysis was conducted using GRANTA Edupack and provides the general information about the material such as strengths and weakness shown in Appendix D. The main benefit of PI is that it has excellent heat resistance [260°C (500°F)] in continuous use, in tandem with having inherent fire-retardance and low smoke emission and excellent heat distortion temperature makes it a prime candidate for PCB. The limitations that Polyimide has is the high cost to produce, with the melt process being very difficult, making the manufacturing process of it be a slower process. It also has a relatively low impact strength, and worse elongation at break which can be a problem during the deployment process.

Alumina

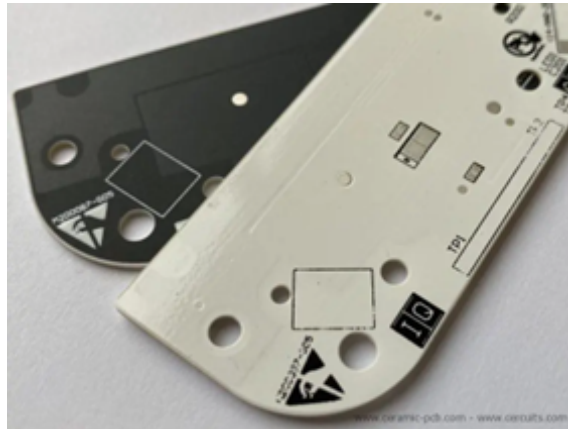


Figure 4.12.: Alumina Oxide PCB [3]

Alumina (Aluminium Oxide or Al_2O_3) is a ceramic that is a chemical compound of aluminium and oxygen, the 96% refers to the purity of the aluminium. A material analysis was also conducted using GRANTA Edupack and is shown in Appendix D. In abrasive environments they can maintain a long service life due to their high hardness and wear resistance, which would be ideal for the space usage because it has one of the extreme environments imaginable. They also have a high-temperature resistance with a high melting point at 2000-2100°C and outstanding thermal stability. It also has excellent corrosion resistance which is ideal for space usage where it can be a corrosive environment. It also is lightweight with its density ranging from 3.69 to 3.73 g/cm³. The disadvantages

of it are the brittleness of the ceramic and can fracture on impact which limits the lifespan in the space usage to mechanical shocks. It is also difficult to machine from the high hardness so initial costs for manufacturing and lead time are higher than other materials [25], [26].

PTFE(Teflon)



Figure 4.13.: PTFE/Teflon sheets [4]

Polytetrafluoroethylene (PTFE) is a synthetic Fluoropolymer they have been known to be chemically inert, low friction properties and has a high heat resistant.

PTFE, also known as Teflon, is renowned for its great electrical characteristics, particularly its low loss tangent and dielectric constant [27]. These characteristics make it an excellent candidate for high-frequency applications, which are common in space communication systems [27]. Furthermore, PTFE is highly resistant to chemicals and outgassing, making it ideal for the hostile space environment [27]. Teflon is also used as a solid lubricant for numerous moving parts in spacecraft because of its resistance to heat and non-stick qualities [28].

From the GRANTA Edupack it has a melting point that ranges from 315-339°C and can operates at its maximum service temperate from 250-270°C which allows the PCB to work in high temperature environments. Because it is chemically inert it is suitable for it to space PCB [29].

Copper Foils

High-performance copper foils are essential in space-grade PCBs to ensure excellent signal integrity and efficient heat dissipation [18]. Copper's excellent electrical and thermal conductivity makes it the ideal material for conductive layers on a PCB. In applications requiring larger current carrying capability, thicker copper traces are frequently used [30]. The quality and thickness of the copper foil are crucial parameters that influence both the



Figure 4.14.: Copper foils [5]

electrical performance and thermal management capabilities of the PCB in the demanding space environment.

Kapton

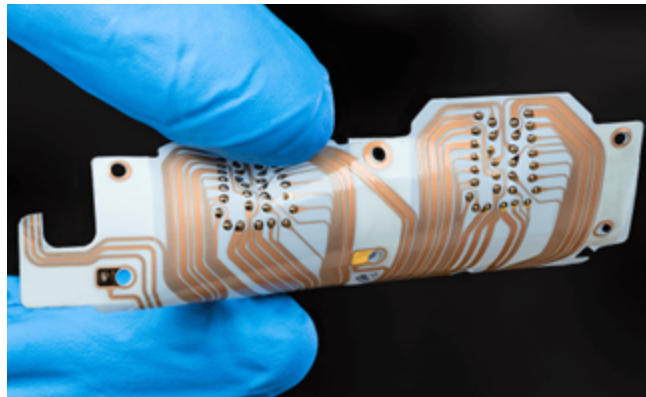


Figure 4.15.: Kapton PCB [6]

Kapton is highly radiation resistant and compatible with harsh conditions. Engineers typically use it to insulate cables and components in high vacuum chambers because it withstands radiation while having minimal influence on instrument base pressure [24]. Kapton, which can withstand temperatures of up to 400°C, can be combined with other materials like gold to create heat-resistant blankets for use in spacecraft. Kapton's flexibility and outstanding performance under harsh temperatures make it an ideal material for a variety of insulation and protection applications in space hardware [24].

Material Selection for PCB

The Comparing the elongation between the polyimide, alumina and PTFE, polyimide has the most ideal value being 75%–80% compared to alumina's 0.07%-0.09% or PTFE's 200%-400%, because having too little elongation can have a major risk of under deformation it will break, and having too much elongation causes the PCB to irreparably warp,

having an in-between ensures it can deform when under forces without breaking. Polyimide has the lowest density which is ideal for having weight limit on the shuttle craft. Polyimide has the highest cost per kg which can be a major restraint on the budget whilst alumina and PTFE are far cheaper in comparison. All 3 have the necessary operating temperature criteria of space temperatures from -200°C to +200°C. From this it is decided that the best material for PCB is polyimide, because it has the required strength, operating temperatures and it has the best middle road on its elongation (%) and flexural modulus making it ideal for space usage.

4.5.5. CubeSat Chassis Material

The standard material that is used in the chassis of the CubeSat are aluminium alloys such as 6061 or 7075, which is to remain lightweight but without sacrificing strength. There's also need to thermal management to it to manage the fluctuations in space, commonly using multi-layer insulation to achieve this. The 4-digit designation represents what type of aluminium it is; the first digit can be 1 to 8 which represents which wrought it is. The second digit is often 0 meaning it is in the base form, any number other than this indicates it has been altered. The third and fourth digits identifies what individual alloys they are. A comparison table was created in GRANTA Edupack to compare all the Aluminium 6061 variants would be the best, and 6061-T651 was found to be the best out of all of them, as seen in the appendix.

Aluminium 6061- T651

Aluminium 6061-T651 has a good strength-to-weight ratio which offers a good balance between the strength and weight without compromising one to a detrimental degree. It's also strong with the tensile strength up to 320 MPa. It is used in many structural applications because it is strong by itself and is lighter than steel making it ideal in the automotive and aerospace industries. It is also highly recyclable and non-toxic so after usage it can be reused and does not cause harm to be in proximity with. It is also not suspectable to stress corrosion cracking making it ideal for space use when external and internal forces are applied towards it.

Aluminium 7075

Aluminium 7075 is one of the strongest aluminium available with a tensile strength listed at 580 MPa making it an ideal material for structural and load-bearing applications. Just like 6061 it is also lightweight with a good strength to weight ratio and highly recyclable. However, it is highly susceptible to stress corrosion cracking which is a major weakness especially for space applications from the external and internal forces applied to it.

6061-T651 vs 7075

In terms of strength Aluminium 7075 is considerably stronger than 6061, this makes 7075 a suitable material for applications requiring high strength such as Construction. However, 6061 is much more flexible with having better ductility making it easier to form weld into shape what the design requires. 6061 also has better resistance in corrosion due to things in space such as atomic oxygen oxidising the metal. And 6061 is cheaper and simpler production process because of its machinability compared to 7075. It is decided that the most suitable for the chassis should be 6061-T651 because of the corrosion resistance, and machinability keeping cost down, with the better ductility to avoid the chassis structure to snap under forces, whilst 7075 is stronger, they already are suitable strength wise in space that it is a moot point.

Emerging Materials and Future Trends

Emerging materials and future trends in space PCB technology are being shaped by advances in materials science and manufacturing techniques that try to solve the unique challenges provided by the space environment. Next-generation materials such as 2D materials, organic electronics, and metamaterials are being investigated for their potential to increase the performance and reliability of space electronics by offering severe temperature resistance, radiation shielding, and enhanced thermal conductivity [31].

Furthermore, hybrid and composite materials, including self-healing polymers and multifunctional carbon fibre composites, are being developed to withstand the extreme conditions of space, such as micrometeorite impacts and electromagnetic interference, thus improving the feasibility and safety of space exploration [32]. All these developments point to a future in which space PCB technology is more integrated, efficient, and capable of meeting the expanding demands of space missions.

4.5.6. Quality Assurance and Reliability Standards in Space PCB Manufacturing

NASA Standards

NASA has comprehensive standards to ensure PCB quality and reliability PCBs used in space missions. NASA-STD-8739.1 defines the workmanship standards for polymeric applications on electrical assemblies, such as conformal coatings used to protect PCBs in defence and aerospace applications [33]. The Goddard Space Flight Centre (GSFC) has released GSFC-STD-8001, which specifies quality assurance standards for the design, procurement, fabrication, and use of high-reliability PCBs in GSFC project mission hardware [34]. GSFC-STD-8002 provides the requirements for the validation of manufacturing processes for printed wiring assemblies using water-soluble fluxes [35]. The NASA PCB

Working Group (PCB WG) is a helpful resource, offering expertise in PCB technology assessment and recommendations for quality assurance measures [27]. NASA generally uses polyimide-based laminates with glass reinforcements in its PCB constructions [36]. The agency also emphasises the necessity of visual acuity testing in accordance with NASA-STD-8739.6 or IPC-QL-653, and PCB inspectors must hold IPC-A-600 Certified IPC Specialist (CIS) accreditation to ensure complete and accurate quality control [34].

ESA Standards

The European Space Agency (ESA) also enforces strict requirements for materials and procedures used in space applications, including PCBs. These standards are extensively described in the European Cooperation for Space Standardisation (ECSS) series. ECSS-Q-ST-70-02C describes the thermal vacuum outgassing test protocols for screening space materials [17]. ECSS-Q-ST-70-10C specifies the requirements for qualified printed circuit boards [37], whereas ECSS-Q-ST-70-60C Corrigendum 1 specifies the requirements for their procurement [38]. Other relevant ECSS standards address a wide range of materials, mechanical parts, and procedures, including cleaning, heat testing, soldering, and crimping [38]. These standards are intended to ensure the reliability and performance of electronic assemblies in the challenging space environment.

IPC Standards

IPC, a global trade group for the electronics industry, has established a number of standards that are commonly used in the production of space-grade PCBs. IPC-2221 is a generic standard that covers practically every area of PCB design [18]. Specific subsection standards are IPC-2222 for rigid boards, IPC-2223 for flex circuits, and IPC-2226 for HDI structures [18]. IPC-6012 specifies the certification and performance standards for rigid PCBs, whereas IPC-6013 accomplishes the same for flexible printed boards [18]. IPC-A-600 specifies the visual inspection standard for PCB acceptability [18]. For surface mount designs, IPC-7351 provides critical guidelines [18].

For military and aerospace applications, IPC Class 3/A, as defined in IPC-6012 Class 3/A, denotes high reliability requirements [39]. Furthermore, the IPC 6012 Space Addendum specifies standards for class 3 boards used in the space and military avionics industries, including requirements to endure vibration, ground testing, and temperature cycling [40].

US Military Standards(MIL-SPEC)

The United States Military has developed its own performance criteria for PCBs used in defence and aerospace applications. MIL-PRF-31032 specifies the requirements for high-reliability, stiff PCBs, whereas MIL-PRF-50884 addresses flexible PCBs [17]. MIL-

PRF-55110 covers stiff PCBs used in military applications [41]. These standards set strict requirements on material selection, design, manufacturing processes, and testing to assure PCB dependability in hostile operating environments [41]. Furthermore, standards such as MIL-STD-810 explain environmental engineering issues for military equipment, while MIL-STD-461 establishes requirements for electromagnetic compatibility [39]. Compliance with MIL-SPEC standards is commonly required for PCBs used in military and aerospace systems.

4.6. Thermal Analysis of the PCB

4.6.1. Hypothesis

The purpose of the thermal analysis is to validate that the Polyimide PCB and the components can operate under the space conditions. The operational temperature of Polyimide minimum is -240°C and the maximum is 260°C . If the components are within the operational temperature range, then it is validated to be operational under dynamic heat conditions, however if it exceeds it, then the PCB material, and the PCB design with the component locations must be altered and reworked. It is expected that the photodiodes area of the PCB to have the most thermal activity, with the lowest thermal activity occurring to the resistors.

4.6.2. Thermal Analysis Parameters

After a PCB CAD model is designed and material selection is completed, the thermal analysis for the PCB can now be conducted. The PCB CAD model was imported into ANSYS workbench using steady-state thermal analysis and a mesh was applied generated to the model to influences the accuracy and convergence of the simulation. Each off the components have their respective materials applied to the model, such as the photodiode with silicon and aluminium, connectors being made of copper, nickel, zinc, amplifiers and resistors made from aluminium, and the PCB being made of polyimide. Then a convection of 22°C was applied to the side of the PCB to simulate the transfer of heat of the PCB from the shuttlecraft it is housed in, assumingly room temperature of the spacecraft is the same as on Earth, it would be 22°C . Each of the components have their respective temperatures when operating. Finally, two tests will be conducted using 200°C and -200°C of radiation applied to the entire PCB model to simulate when the PCB is facing to the sun, and when the PCB is in the shadows of celestial bodies respectively.

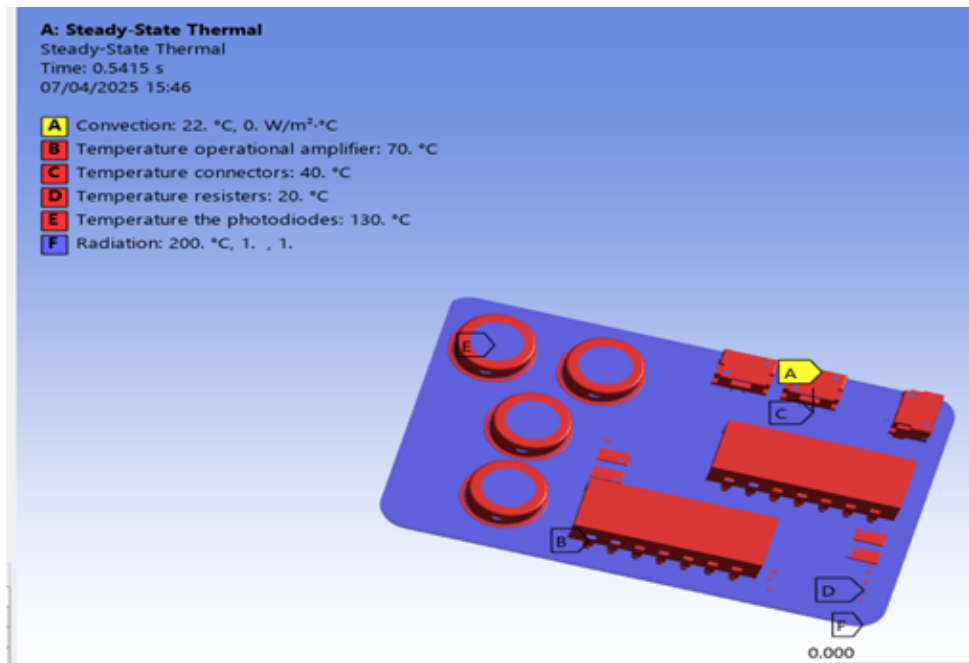


Figure 4.16.: PCB model with Parameters applied

4.6.3. Thermal results

4.6.4. Finite Analysis Evaluation 1 - Under 200 °C in space

The results for the PCB when facing towards the sun depicts the most heat being towards outside of the photodiodes area and the cooler parts are around the other components. As Figure 4.17 shows the maximum temperature experienced is 199.35 °C and the minimum temperature is –31.168 °C, this shows that the PCB can be operable when facing towards the Sun.

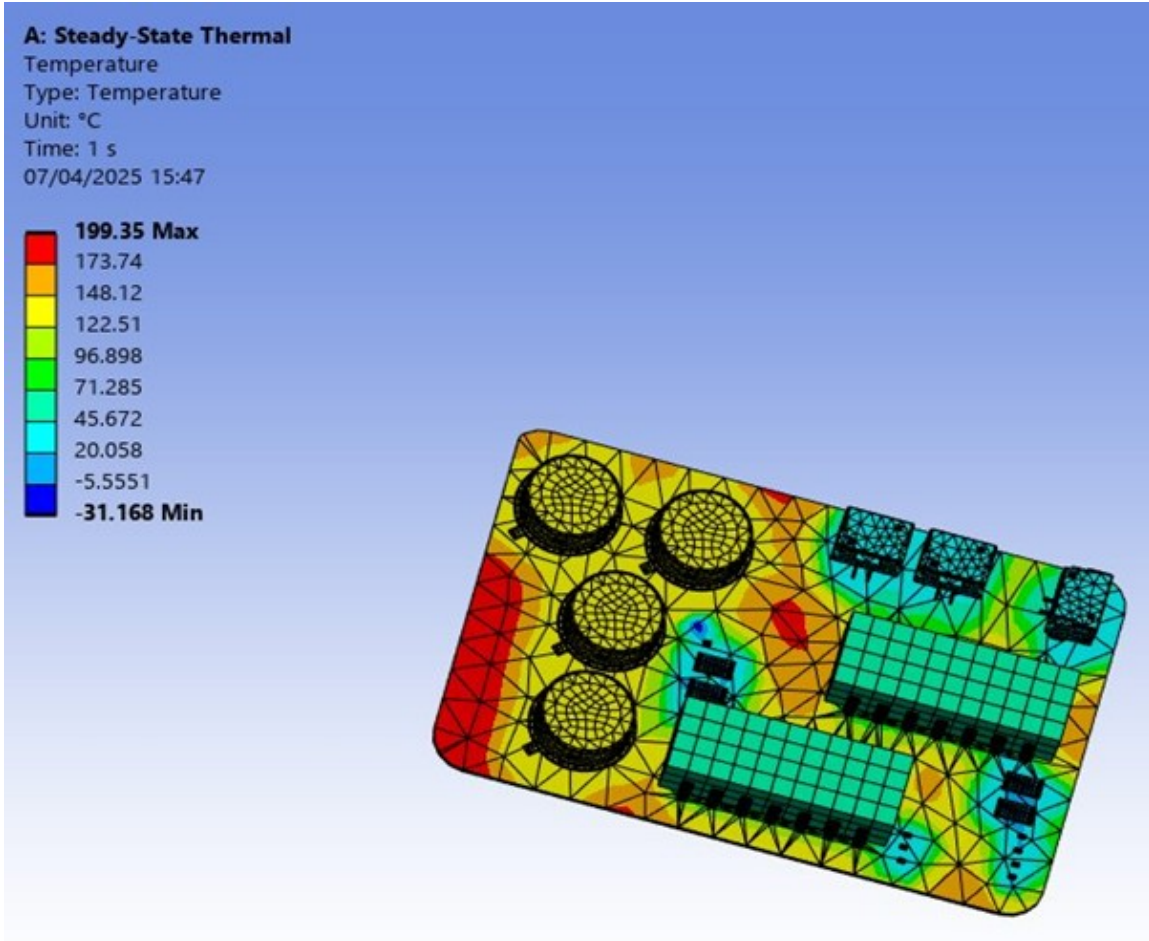


Figure 4.17.: Results under 200 °C radiation

Finite Analysis Evaluation 2 - Under -200°C in space

The results for the PCB, when it is in the shadows of a celestial body depicts the most heat coming from the photodiodes themselves which is to be expected as it creates the most heat in the PCB components followed by the amplifiers then connectors. As Figure 4.18 shows the maximum temperature experienced is 136°C and the minimum temperature is -173.83°C , this shows that the PCB can be operable when in the shadow of a celestial body.

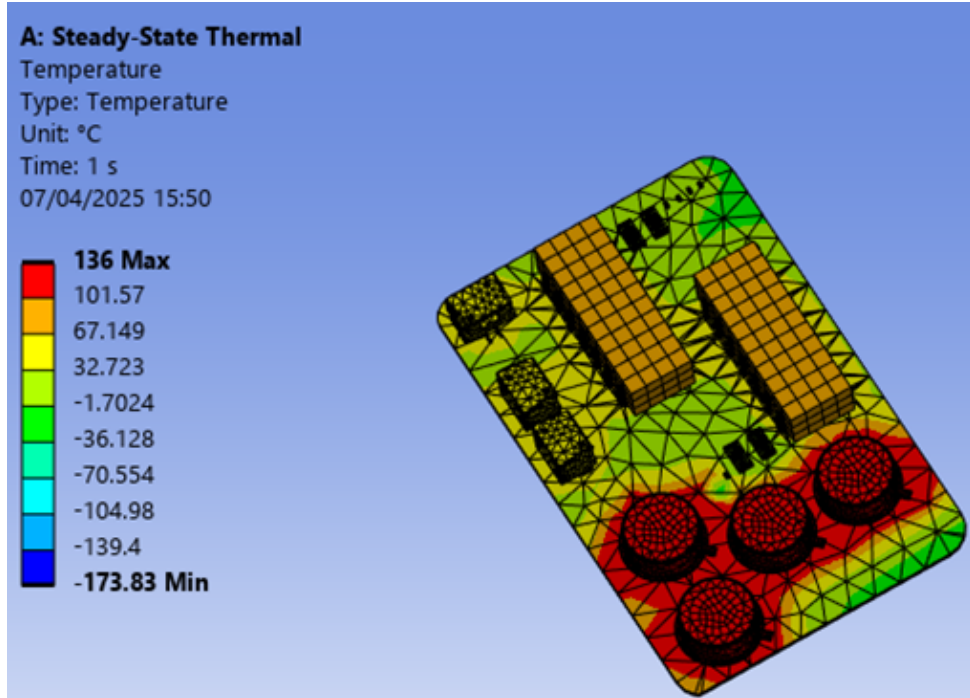


Figure 4.18.: Results under -200°C radiation

4.6.5. Results Evaluation

The results shown for both under 200°C and -200°C radiation shows that the PCB is operable under the harsh thermal conditions in space. That validates the design of the PCB and their component placements, and the material selection. The polyimide having about a clearance when facing the sun at 60°C and when in the shadows of a celestial object at -66°C shows that it would not be on the brink of melting or freezing during operation. The next step would be analysis the stresses and forces at work in space, unfortunately, a mechanical analysis of the stress cannot be conducted because it requires further work with the complete work of the entirety of the CubeSat chassis and all the power source such as the solar panels.

4.7. CubeSat Chassis Design

For the purposes of visualization, there were 2 potential designs for the CubeSat chassis. The CubeSat chassis were design dependant on where the PCB would be mounted. The first CubeSat chassis design was taken from GrabCAD.com and an aperture is mounted to this design to show where they would be mounted. The second CubeSat chassis was based on a design found online and recreated as much as possible, however this did not have any measurements given so dimensions were assumed.

4.7.1. CubeSat Chassis Design 1

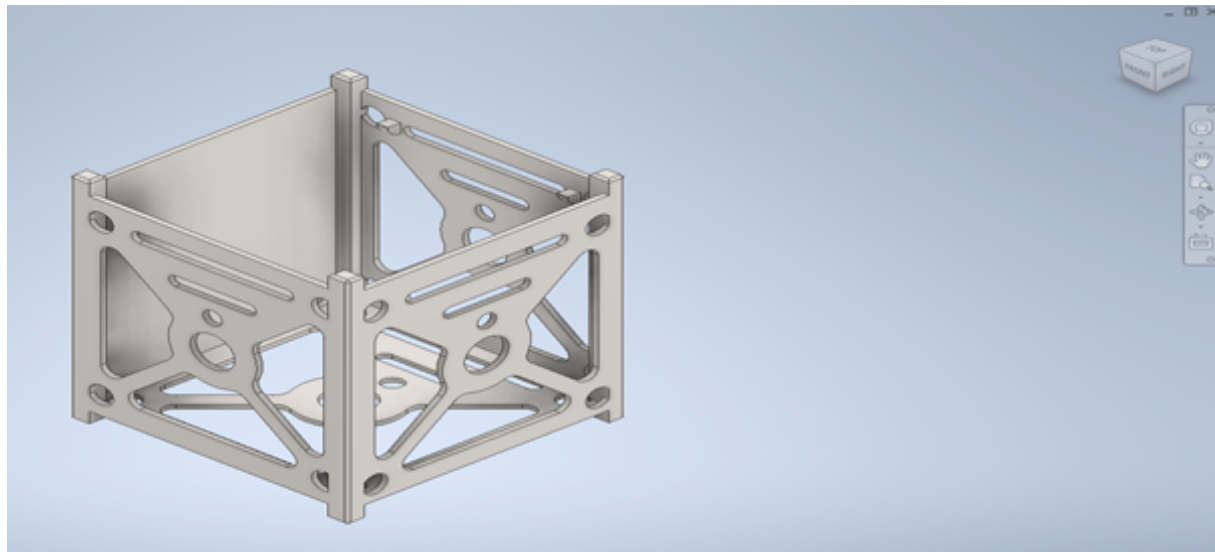


Figure 4.19.: Front view of the first CubeSat chassis design

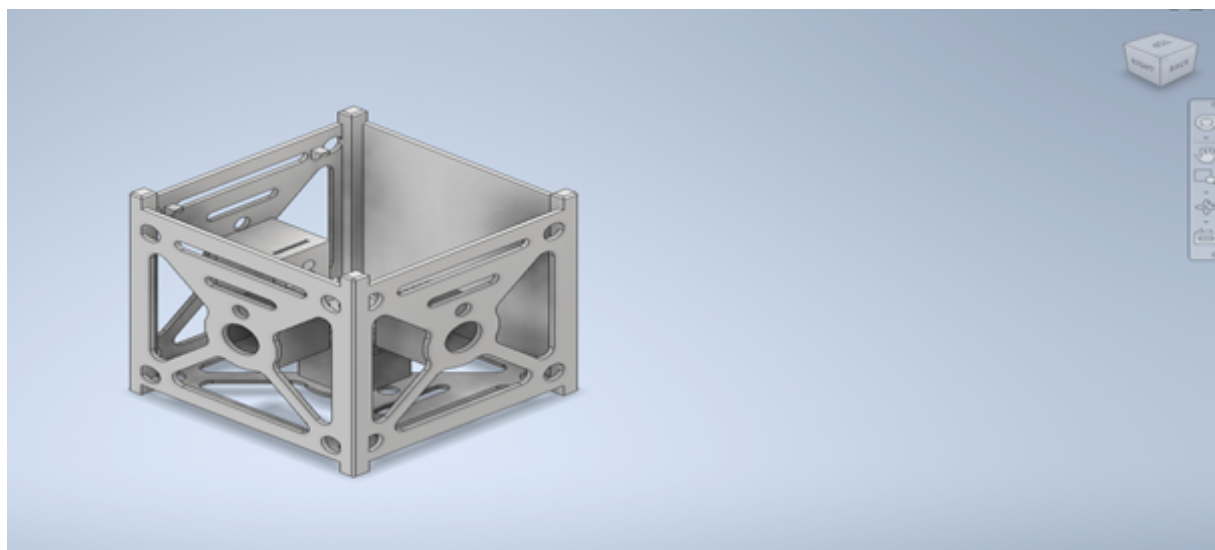


Figure 4.20.: Angular view of the first CubeSat chassis design

The first design taken from <https://grabcad.com/library/cubesat-1u-5> as seen in Figure 4.19 has exposed holes made to allow for easy removal, the circular holes at the centre are to let the light to expose to the aperture where the PCB photodiodes are located. The software used to show these are AutoCAD Inventor, with a different angle and the aperture shown in Figure 4.20.

4.7.2. CubeSat Chassis Design 2

The second hypothetical design is a much more basic skeleton frame made to house the aperture as seen below in Figure 4.21 and Figure 4.22.



Figure 4.21.: Front view of 1U Cubesat Skeleton Chassis



Figure 4.22.: Angular view of 1U Cubesat Skeleton Chassis

This was recreated in inventor with rough estimation on the thickness of the PCBs and skeletons itself and the apertures. The PCBs are mounted on top of each other compared to being the aperture housing the PCB mounted on each side of the CubeSat, the PCB cannot be more than 96×96 mm. As seen below in Figure 4.23 and Figure 4.24, are the CubeSat Chassis with and without the PCBs, additional angles and drawings are found in the appendix.

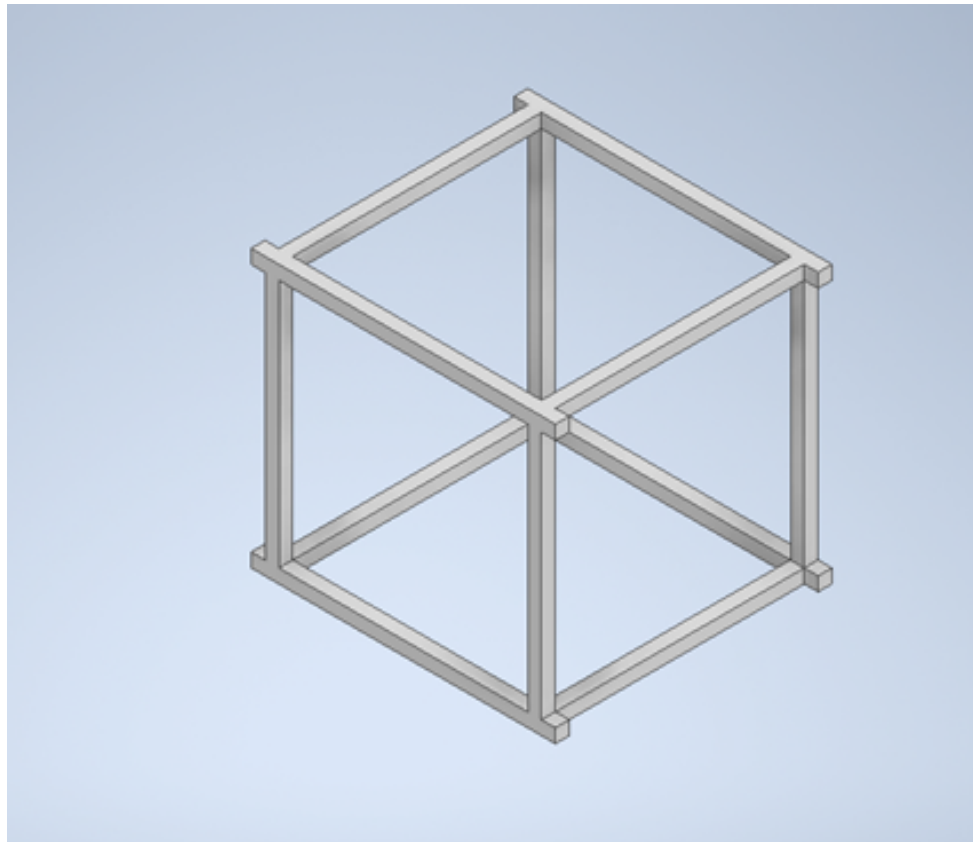


Figure 4.23.: Second chassis design without PCBs

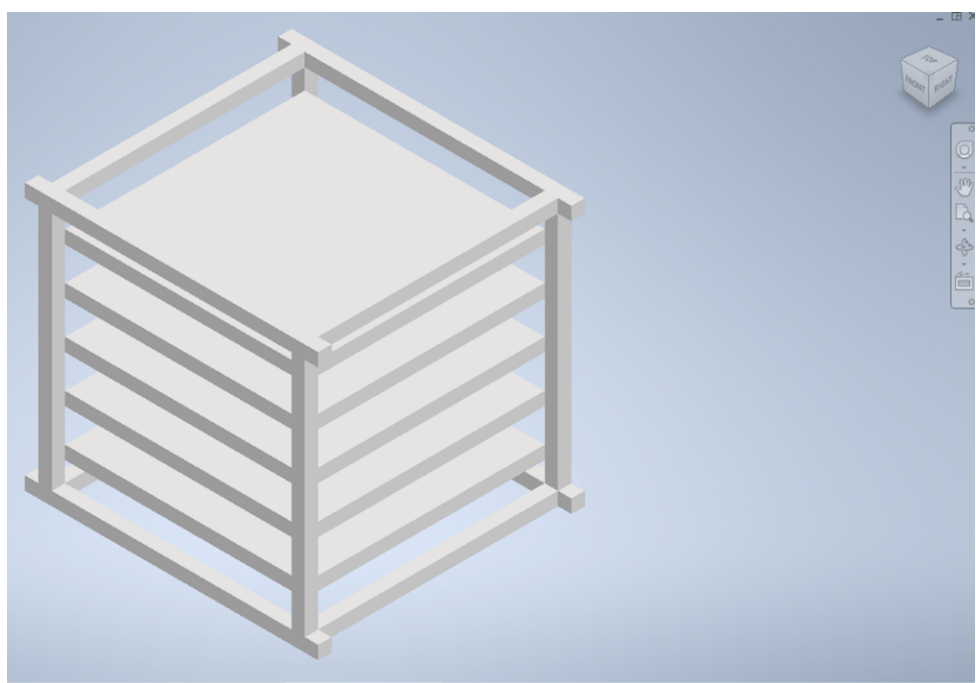


Figure 4.24.: Chassis with the aperture

5. Results

5.1. Sensor Characterization

TO FINISHTO FINISHTO FINISHTO FINISHTO FINISHTO FINISHTO FINISH focus on the fundamental properties and performance of your photodiodes themselves, distinct from the other subsections. Here are some key elements that would belong specifically under SensorCharacterization:

Basic Photodiode Electrical Characteristics:

Dark current measurements Junction capacitance I-V characteristics in different lighting conditions Spectral response profiles (sensitivity vs. wavelength)

Individual Sensor Benchmarking:

Performance comparison between the 4 photodiodes (matching/differences) Responsivity measurements (A/W) Quantum efficiency calculations Detection threshold levels

SNR!

Response Linearity:

Measurements showing linear range of the photodiodes Saturation point characterization Recovery time from saturation

Temperature Dependency:

Performance drift with temperature Baseline shift measurements Temperature compensation data

Aging/Stability Tests:

Long-term drift measurements Repeatability of measurements over time

This section should focus on the inherent properties of the photodiodes themselves - essentially providing the baseline characterization data that underpins all the other analysis. The other sections then build on this foundation by examining how these sensors perform when integrated into the complete system with amplification, angular positioning, enclosure effects, etc.

5.2. Amplification Performance

This section provides results of the amplifier performance.

5.3. Photodiode Angular Response

This section discusses the results of the response of the solar sensor to angular changes of the light source.

5.4. Enclosure Effectiveness

This section discusses the effectiveness of the Photodiode enclosure.

5.5. Data Acquisition System Evaluation

This section provides results related to the Arduino DAQ.

5.6. System Performance Analysis

5.6.1. Operational Constraints Identified

5.6.2. Environmental Factors Impact

5.6.3. System Stability and Repeatability

5.6.4. Recommendations for Improvement

5.7. Comparative Analysis

This section compares the simulation with the prototype results.

5.7.1. Breadboard vs. Stripboard Results

5.7.2. Iteration Improvements Analysis

5.7.3. Performance Against Design Requirements

The performance ...

5.7.4. Design Evolution Assessment

The what now?

5.8. System Limitations And Considerations

This section discusses the limitations and future work.

5.8.1. Angle accuracy

6. Conclusions

7. Future Work

Mention: methods to avoid detecting sun reflections off the moon and earth (such as light intensity or light source width if possible).

Bibliography

- [1] A. V. Oppenheim and R. W. Schafer, *Discrete-Time Signals and Systems*. India: Pearson, 2013.
- [2] 86PCB, “Fr-4 pcb: Material properties, thickness selection, and application guide - 86pcb,” Jul 19 2024. [Online]. Available: <https://86pcb.com/blog/fr-4-pcb-material-properties-thickness-selection-and-application-guide/>
- [3] CERCuits, “Aluminum oxide pcb (alumina),” 2025. [Online]. Available: <https://ceramic-pcb.com/aluminum-oxide-pcb-al2o3/>
- [4] Imimg, “Teflon/ptfe sheets,” 2025. [Online]. Available: <https://3.imimg.com/data3/JP/YY/MY-1996077/teflon-ptfe-sheets.jpg>
- [5] V. Solutions, “Copper foil,” 2022. [Online]. Available: <https://viin-solution.com/images/newimage/Copper-Foil2.jpg>
- [6] Goodfellow, “Kapton,” 2025. [Online]. Available: https://www.goodfellow.com/media/wysiwyg/kapton-image-2_1_.png
- [7] J. Puig-Suari and C. Turner, “Development of the standard cubesat deployer and a cubesat class picosatellite,” 2001.
- [8] K. S. Balaji, B. S. Anand, P. M. Reddy, V. C. B, M. D. P. Lingam, and V. K, “Studies on attitude determination and control system for 1u nanosatellite,” *ICCPCT*, pp. 616–625, 2023.
- [9] I. Lopez-Calle and A. I. Franco, “Comparison of cubesat and microsat catastrophic failures in function of radiation and debris impact risk,” *Scientific Reports*, vol. 13, no. 1, -01-07 2023.
- [10] P. Ortega, G. López-Rodríguez, J. Ricart, M. Domínguez, L. M. Castañer, J. M. Quero, C. L. Tarrida, J. García, M. Reina, A. Gras, and M. Angulo, “A miniaturized two axis sun sensor for attitude control of nano-satellites,” p. 1623, -10 2010.
- [11] G. Keiser, *Fiber Optic Communications*, 1st ed. Singapore: Springer, 2021.

- [12] Atmel, “Atmega328p 8-bit avr microcontroller with 32k bytes in-system programmable flash datasheet,” 2015. [Online]. Available: https://ww1.microchip.com/downloads/en/DeviceDoc/Atmel-7810-Automotive-Microcontrollers-ATmega328P_Datasheet.pdf
- [13] T. S. community, “butter scipy v1.15.2 manual.” [Online]. Available: <https://docs.scipy.org/doc/scipy/reference/generated/scipy.signal.butter.html#scipy.signal.butter>
- [14] ——, “filtfilt — scipy v1.15.2 manual,” 2025. [Online]. Available: <https://docs.scipy.org/doc/scipy/reference/generated/scipy.signal.filtfilt.html>
- [15] N. I. Shopov, S. Hannisse, and S. Gupta, “Renewable energy demonstrator (red),” Glasgow Caledonian University, Tech. Rep., 2022.
- [16] G. L. G. Burbui, U. Reggiani, and L. Sandrolini, “Prediction of low-frequency electromagnetic interferences from smps,” *ISEMC*, vol. 2, pp. 472–477, 2006.
- [17] W. Leverett, “Satellite technology: Pcb in space exploration and communications | abl circuits,” Feb 5 2024. [Online]. Available: <https://www.ablcircuits.co.uk/blog/pcb-satellite-exploration-communication/>
- [18] C. D. Systems, “Applying ipc pcb design standards | cadence,” 2025. [Online]. Available: <https://resourcespcb.cadence.com/blog/applying-ipc-pcb-design-standards-cadence>
- [19] Proto-Electronics, “Space-grade pcbs: challenges in designing electronics for extreme environments,” Jan 11 2024. [Online]. Available: <https://youtu.be/ZgLfodLlgcI>
- [20] 911EDA, “Space pcb design challenges: Engineering for the cosmos,” 2024. [Online]. Available: <https://www.911eda.com/articles/space-pcb-design-challenges/>
- [21] Gatema, “Challenges in pcb design for space applications | gatema,” Jul 17 2024. [Online]. Available: <https://www.gatemapcb.com/challenges-in-pcb-design-for-space-applications/>
- [22] P. Directory, “Understanding pcb design techniques for space-qualified applications. - pcb directory,” Apr 9 2025. [Online]. Available: <https://www.pcbdirectory.com/community/understanding-pcb-design-techniques-for-space-qualified-applications>
- [23] F. Circuits, “Pcbs for space: Ensuring reliability in space applications,” Feb 21 2025. [Online]. Available: <https://www.fscircuits.com/pcbs-for-space/>

- [24] M. E. Tech, “Making a material difference in aerospace and defense electronics,” December 1 2024. [Online]. Available: <https://www.mobilityengineeringtech.com/component/content/article/52137-making-a-material-difference-in-aerospace-defense-electronics>
- [25] Mascera-Tec, “Advantages and disadvantages of alumina ceramic,” Website, n.d., accessed: 15 April 2025. [Online]. Available: <https://www.mascera-tec.com/news/advantages-and-disadvantages-of-alumina-ceramic>
- [26] V. Ceramics, “Advantages and disadvantages of alumina ceramics,” Website, n.d., accessed: 15 April 2025. [Online]. Available: <https://vhandy.com/pros-and-cons-of-alumina-ceramics/>
- [27] C. D. Systems, “Designing reliable pcbs for space applications,” 2025. [Online]. Available: <https://resourcespcb.cadence.com/blog/designing-reliable-pcb-for-space-applications>
- [28] F. Lou, “How to select satellite components that can withstand space,” Feb 5 2023. [Online]. Available: <https://revolutionized.com/satellite-components/>
- [29] R. PCB, “Introduction to ptfe teflon,” LinkedIn post, September 14 2023. [Online]. Available: <https://www.linkedin.com/pulse/what-ptfe-teflon-material-pcb-rayming-techonloy>
- [30] S. international, “Design guidelines for military and aerospace pcbs,” May 1 2022. [Online]. Available: <https://www.mobilityengineeringtech.com/component/content/article/45799-design-guidelines-for-military-and-aerospace-pcbs>
- [31] A. E. Ona-Olapo, T. D. Iluyomade, T. M. Olatunde, and O. P. Igbinenikaro, “Next-generation materials for space electronics: A conceptual review,” *Open Access Research Journal of Engineering and Technology*, vol. 6, no. 2, pp. 51–62, Apr 30 2024. [Online]. Available: <https://oarjpublication.com/journals/oarjet/sites/default/files/OARJET-2024-0020.pdf>
- [32] J. C. Ince, M. Peerzada, L. D. Mathews, A. R. Pai, A. Al-Qatatsheh, S. Abbasi, Y. Yin, N. Hameed, A. R. Duffy, A. K. Lau, and N. V. Salim, “Overview of emerging hybrid and composite materials for space applications,” *Advanced Composites and Hybrid Materials*, vol. 6, no. 4, -06-26 2023.
- [33] S. C. Systems, “Nasa inspection criteria for conformal coating,” Mar 10 2021. [Online]. Available: <https://scscoatings.com/newsroom/blog/nasa-inspection-criteria-for-conformal-coating/>

- [34] G. S. F. Centre, “Standard quality assurance requirements for printed circuit boards (gsfc-std-8001),” Nov 21 2019. [Online]. Available: <https://standards.nasa.gov/standard/GSFC/GSFC-STD-8001>
- [35] ——, “Standard quality assurance for use of water soluble flux(gsfc-std-8002),” Mar 09 2015. [Online]. Available: <https://standards.nasa.gov/sites/default/files/standards/GSFC/Baseline/0/GSFC-STD-8002.pdf>
- [36] C. D. Systems, “Designing reliable pcbs for space applications,” 2025. [Online]. Available: <https://resourcespcb.cadence.com/blog/designing-reliable-pcbs-for-space-applications>
- [37] ECSS, “Ecss-q-st-70-02c,” Nov 15 2008. [Online]. Available: <https://ecss.nl/standard/ecss-q-st-70-02c-thermal-vacuum-outgassing-test-for-the-screening-of-space-materials/>
- [38] ——, “List of published ecss standards (long) | european cooperation for space standardization,” 2019. [Online]. Available: <https://ecss.nl/list-of-published-ecss-standards-long/>
- [39] S. international, “Design guidelines for military and aerospace pcbs,” May 1 2022. [Online]. Available: <https://www.mobilityengineeringtech.com/component/content/article/45799-design-guidelines-for-military-and-aerospace-pcbs>
- [40] R. Shashikanth, “5 military grade pcb design rules | sierra circuits,” Jan 5 2021. [Online]. Available: <https://www.protoexpress.com/blog/military-grade-pcb-design-rules-considerations/>
- [41] C. D. Systems, “Pcb design for military and aerospace applications,” Oct 9 2024. [Online]. Available: <https://resourcespcb.cadence.com/blog/2024-pcb-design-for-military-aerospace-applications>

A. Appendix - DAQ Code

A.1. Arduino DAQ full code

A.1.1. Arduino C++ Code

```
1  /*
2   * Reads 4 analog inputs (0-5V) for recording_dur seconds
3   * Streams data to PC while recording
4   */
5   // change to true to print debug messages on Serial Monitor
6   // printing debug lines impacts transmission speed and messes csv
7   // do not leave on during measurements!
8   bool debug = false;
9
10  const int analogInputs[] = {A0, A1, A2, A3};
11
12
13  // set up the global variables
14  unsigned long start_time;
15  const unsigned long recording_dur = 5000; // 25 seconds in
milliseconds (ENSURE python code is greater than this)
16  unsigned long last_sample_time = 0;
17  const unsigned long min_samp_interval = 2; // Sample every 2ms (
adjust for stability)
18  bool recording = false;
19  int sample_count = 0;
20
21 void setup() {
22     // serial communication at 115200 bps
23     Serial.begin(115200);
24
25     // Set pins as input
26     for (int i = 0; i < 4; i++) {
27         pinMode(analogInputs[i], INPUT);
28     }
29
30     // Optimize ADC for faster sampling
31     // Set ADC prescaler to 16 (default is 128)
32     //
```

```

33     // Bit: 7:enable; 6: initiate a conversion 5:
34     //
35     ADCSRA = (ADCSRA & 0xF8) | 0x04;
36
37     // Wait for serial connection to establish
38     delay(1000);
39
40     // Send ready message
41     Serial.println("ARDUINO_DAQ_READY");
42 }
43
44 void loop() {
45     // Check if we received a command
46     if (Serial.available() > 0) {
47         String command = Serial.readStringUntil('\n');
48         command.trim();
49
50         if (command == "START") {
51             if(debug) Serial.println("received START command");
52
53             // Clear any remaining data in serial buffer
54             while (Serial.available()) {
55                 Serial.read();
56             }
57
58             // Reset sample counter
59             sample_count = 0;
60
61             // Send header once
62             Serial.println("Sample,Time(ms),A0(V),A1(V),A2(V),A3(V)");
63
64             // Start recording
65             recording = true;
66             start_time = millis();
67             last_sample_time = start_time;
68
69             // Send confirmation
70             Serial.println("RECORDING_STARTED");
71         }
72     }
73
74     // If we're recording, collect and send data immediately
75     if (recording) {
76         if(debug) Serial.println("Recording!");
77         unsigned long currentTime = millis();
78         unsigned long elapsed_time = currentTime - start_time;
79

```

```

80     // Check if we're still within the recording period
81     if (elapsed_time <= recording_dur) {
82         if(debug) Serial.println("elapsed time << duration");
83         // Only sample at the specified interval
84         if (currentTime - last_sample_time >= min_samp_interval) {
85             last_sample_time = currentTime;
86
87             // Increment sample counter
88             sample_count++;
89
90             // Start building the output string
91             String data_string = String(sample_count) + "," + String(
92             elapsed_time);
93
94             // Multiplex through the four inputs sequentially
95             for (int i = 0; i < 4; i++) {
96                 if(debug) Serial.println("reading input: " + String(i));
97                 int raw_value = analogRead(analogInputs[i]);
98                 float voltage = raw_value * (5.0 / 1023.0);
99                 data_string += "," + String(voltage, 3);
100            }
101
102            // Send the complete data string at once
103            Serial.println(data_string);
104        }
105    } else {
106        // End of recording
107        recording = false;
108
109        // Send notification that recording is complete
110        Serial.println("RECORDING_COMPLETE");
111        Serial.print("SAMPLES_COLLECTED:");
112        Serial.println(sample_count);
113        Serial.println("END_OF_DATA");
114    }
115}
116

```

Listing A.1: C++ Code on Arduino

A.1.2. PC-side Python Serial Receive Script

```

1 import serial
2 import time
3 import matplotlib.pyplot as plt
4 import pandas as pd

```

```

5      import os
6      import numpy as np
7      from scipy import signal
8
9      def apply_lowpass_filter(data, fs):
10         """Apply a 4-pole low-pass Butterworth filter with 5Hz cutoff"""
11         cutoff_freq = 2.0
12         filter_order = 4
13
14         nyquist = 0.5 * fs
15         normal_cutoff = cutoff_freq / nyquist
16         # analog=False implies bilinear Transformation
17         b, a = signal.butter(filter_order, normal_cutoff, btype='low',
18         analog=False)
19         filtered_data = signal.filtfilt(b, a, data)
20
21     return filtered_data
22
23     # Load data from CSV, apply a 4-pole low-pass filter, and save the
24     # filtered data
25     def filter_and_save_data(filename):
26
27         # Read the CSV data to pandas DataFrame
28         # It knows what are the column names
29         df = pd.read_csv(filename)
30
31         # Clean the dataframe - convert all columns to numeric
32         for col in df.columns:                      # v - write NaN where it
33             can't convert to number (in teh data, not column names)
34             df[col] = pd.to_numeric(df[col], errors='coerce')
35
36         # remove rows with NaN (not a number)
37         df = df.dropna()
38
39         # Samples not at exact distance from each other
40         # Calculate the sampling frequency (median of differences)
41         # numpy.diff to get the difference between samples
42         time_diffs = np.diff(df['Time(ms)'])
43         # numpy.median to get the median
44         median_time_diff = np.median(time_diffs) # in milliseconds
45         fs = 1000.0 / median_time_diff # Convert to Hz
46
47         # Filter each analog channel:
48         # ID column head for each channel
49         analog_channels = ['A0(V)', 'A1(V)', 'A2(V)', 'A3(V)']
50         # take each channel one at a time
51         for channel in analog_channels:

```

```

49         # if name matches a column name
50         if channel in df.columns:
51             # add a new column _filtered , and send the array
52             # containing all the raw values to
53             # have them filtered , and save them in the new _filtered
54             # column
55             df[f"{channel}_filtered"] = apply_lowpass_filter(df[
56             channel].values , fs)
57
58             # Save the pandas Dataframe with filtered columns to a new CSV
59             file
60             filtered_filename = f"{os.path.splitext(filename)[0]}_filtered.
61             csv"
62             df.to_csv(filtered_filename , index=False)
63
64             return filtered_filename
65
66             #
67             # Plot the DAQ data with original and filtered signals overlapped
68             #
69             def plot_data(filename):
70
71                 # Read the CSV data with pandas
72                 df = pd.read_csv(filename)
73
74                 # Initialize an empty list to store our analog channel names
75                 analog_channels = []
76
77                 # Look through all column names in the DataFrame
78                 for col in df.columns:
79                     # the column name starts with 'A'
80                     if col.startswith('A'):
81                         # the column name ends with '(V)'
82                         if col.endswith('(V)'):
83                             # the column name does NOT contain '_filtered'
84                             if '_filtered' not in col:
85                                 # add this column name to our list
86                                 analog_channels.append(col)
87
88                 # Create color cycle for different channels
89                 colors = ['blue' , 'green' , 'red' , 'purple']
90
91                 # Create a single plot with all channels overlapping
92                 plt.figure(figsize=(14, 8))
93
94                 # Plot original data (semi-transparent)
95                 for i, channel in enumerate(analog_channels):

```

```

91         color = colors[i % len(colors)]
92         plt.plot(df['Time(ms)'], df[channel], label=f'{channel}
93 Original',
94             linewidth=1.5, alpha=0.4, color=color, linestyle='--'
95 )
96
97     # Plot filtered data (solid lines)
98     for i, channel in enumerate(analog_channels):
99         filtered_channel = f'{channel}_filtered'
100        if filtered_channel in df.columns:
101            color = colors[i % len(colors)]
102            plt.plot(df['Time(ms)'], df[filtered_channel], label=f'{channel} Filtered',
103                 linewidth=2.5, color=color, linestyle='--')
104
105    # Set the y-axis range from 0 to 5V
106    plt.ylim(0, 5)
107
108    # Add labels and title
109    plt.xlabel('Time (ms)')
110    plt.ylabel('Voltage (V)')
111    plt.title('Arduino DAQ - 4-Channel Readings with 4-Pole 5Hz Low-
112 Pass Filter')
113    plt.legend()
114    plt.grid(True)
115
116    # Add data summary
117    duration = df['Time(ms)'].max() - df['Time(ms)'].min()
118    sample_count = len(df)
119    sample_rate = sample_count/(duration/1000) if duration > 0 else
120    0
121
122    info_text = f'Data summary:\n' \
123                f'Duration: {duration:.1f} ms\n' \
124                f'Samples: {sample_count}\n' \
125                f'Sample rate: {sample_rate:.1f} Hz\n' \
126                f'Filter: 4-pole Butterworth, 5Hz cutoff'
127
128    plt.figtext(0.02, 0.02, info_text, fontsize=10,
129                bbox=dict(facecolor='white', alpha=0.8))
130
131    # Save the plot
132    plot_filename = f'{os.path.splitext(filename)[0]}_plot.png'
133    plt.savefig(plot_filename, dpi=300, bbox_inches='tight')
134
135    # Show the plot
136    plt.tight_layout()

```

```

133     plt.show()
134
135     def main():
136
137         # ASk if to plot or measure
138         what_to_do = int(input("Record new measurement (1) or plot
existing (2): "))
139
140         # User selected to plot old csv
141         if(what_to_do == 2):
142             plot_data(input("Insert the name of the csv: "))
143
144
145         # User selected to record new measurement
146         elif(what_to_do == 1):
147             # Use a default port (COM3 for Windows, modify as needed)
148             default_port = "COM3" # Change to match your system
149
150             print(f"Using port: {default_port}")
151
152             # Configure serial port
153             try:
154                 ser = serial.Serial(default_port, 115200, timeout=2)
155                 print("Connected to Arduino!")
156             except serial.SerialException:
157                 print(f"Error: Could not open port {default_port}")
158                 print("Please modify the default_port variable in the
script.")
159             return
160
161             time.sleep(2) # Wait for Arduino to reset
162
163             # Flush buffers
164             ser.reset_input_buffer()
165             ser.reset_output_buffer()
166
167             # Wait for Arduino ready
168             print("Waiting for Arduino to be ready...")
169             ready = False
170             timeout = time.time() + 10 # don't wait too long
171
172             while not ready and time.time() < timeout:
173                 line = ser.readline().decode('utf-8', errors='ignore').
strip()
174                 if line == "ARDUINO_DAQ_READY":
175                     ready = True
176                     print("Arduino is ready!")

```

```

177
178     if not ready:
179         print("Timed out waiting for Arduino. Make sure it's
properly connected.")
180         ser.close()
181         return
182
183     # Create a filename for this recording session
184     filename = f"arduino_daq_data_{time.strftime('%Y%m%d_%H%M%S
')}.csv"
185
186     print(f"Starting data recording to {filename}...")
187     print("Press Ctrl+C to stop if needed.")
188
189     with open(filename, 'w', newline='') as file:
190         # Send start command
191         ser.write(b"START\n")
192
193         recording = True
194         data_lines = 0
195
196         # Start time for timeout
197         start_time = time.time()
198         timeout_duration = 15 # seconds
199
200         while recording and (time.time() - start_time) <
timeout_duration:
201             if ser.in_waiting:
202                 line = ser.readline().decode('utf-8', errors='
ignore').strip()
203
204                 if "RECORDING_COMPLETE" in line:
205                     recording = False
206                     print("Recording complete!")
207                 elif "END_OF_DATA" in line:
208                     pass
209                 elif line:
210                     # Write the line to the file
211                     file.write(line + '\n')
212                     data_lines += 1
213
214                     # Show progress occasionally
215                     if data_lines % 100 == 0:
216                         print(f"Recorded {data_lines} data
points...")
217
218             # Close the serial port

```

```

219         if ser.is_open:
220             ser.close()
221             print("Serial port closed.")
222
223             print(f"Recorded {data_lines} lines of data.")
224
225             # Process the data
226             print("Applying filters to data...")
227             filtered_filename = filter_and_save_data(filename)
228             print(f"Filtered data saved to {filtered_filename}")
229
230             print("Generating plot...")
231             plot_data(filtered_filename)
232             print("Done!")
233
234         else:
235             print("Wrong Choice. Goodbye!")
236             exit()
237     if __name__ == "__main__":
238         try:
239             main()
240         except KeyboardInterrupt:
241             print("\nProgram terminated by user.")

```

Listing A.2: Python Serial Receive Script

B. Appendix - Software Model Code

B.1. Section 1 Title

B.1.1. subsectiontitle

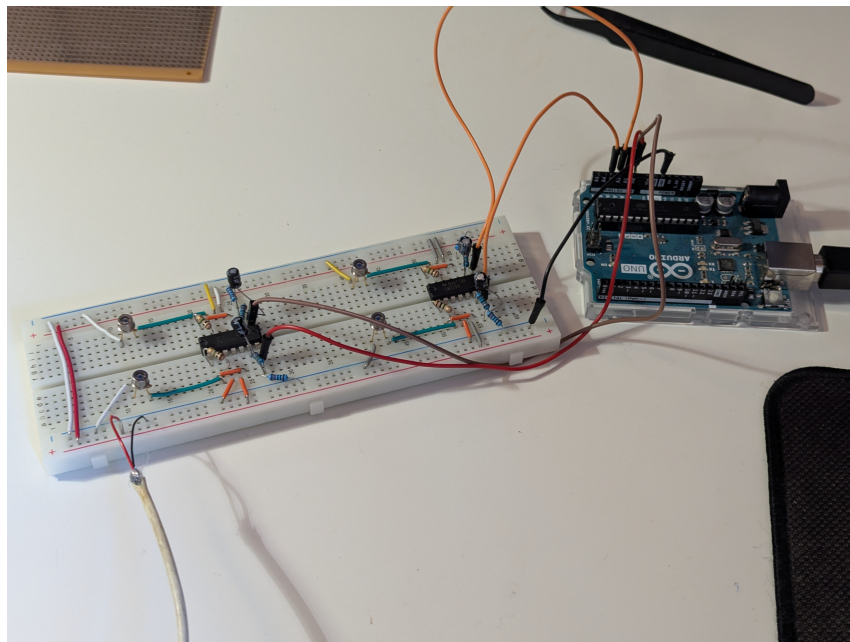
B.2. Section 2 Title

B.2.1. subsectiontitle

C. Appendix - Photos of Lab Work

C.1. Prototype Images

C.1.1. BreadBoard Prototype



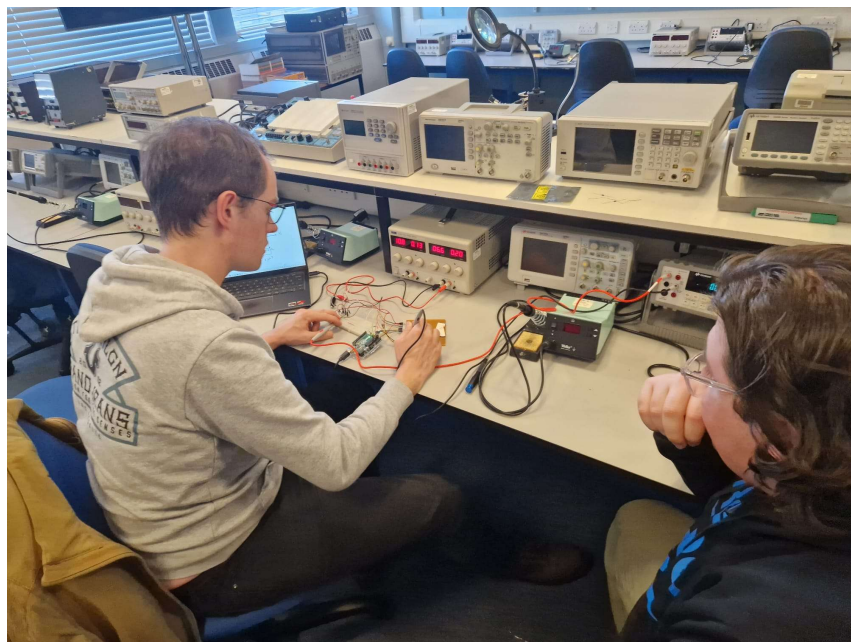
Initial BreadBoard Prototype of the Photodiode Circuit

C.1.2. Building the Prototype

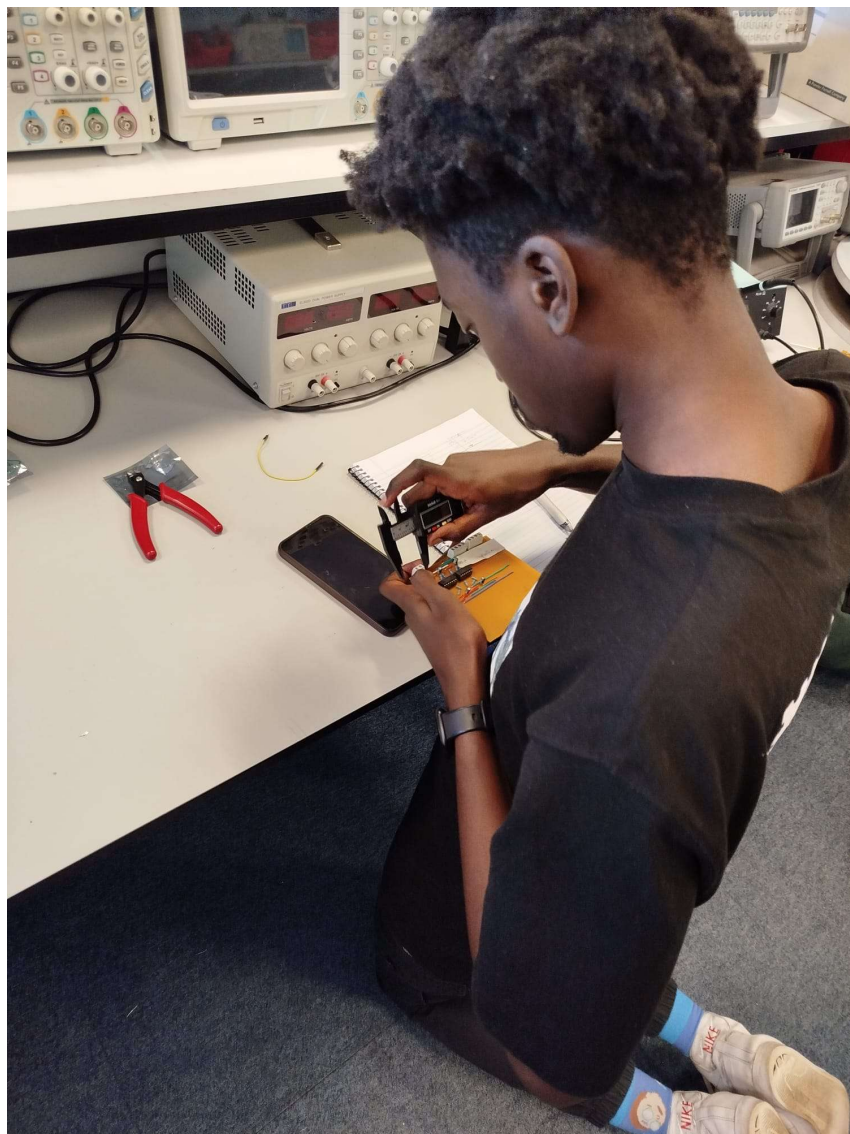
C.1.3. Prototype Testing

C.1.4. RED testbench

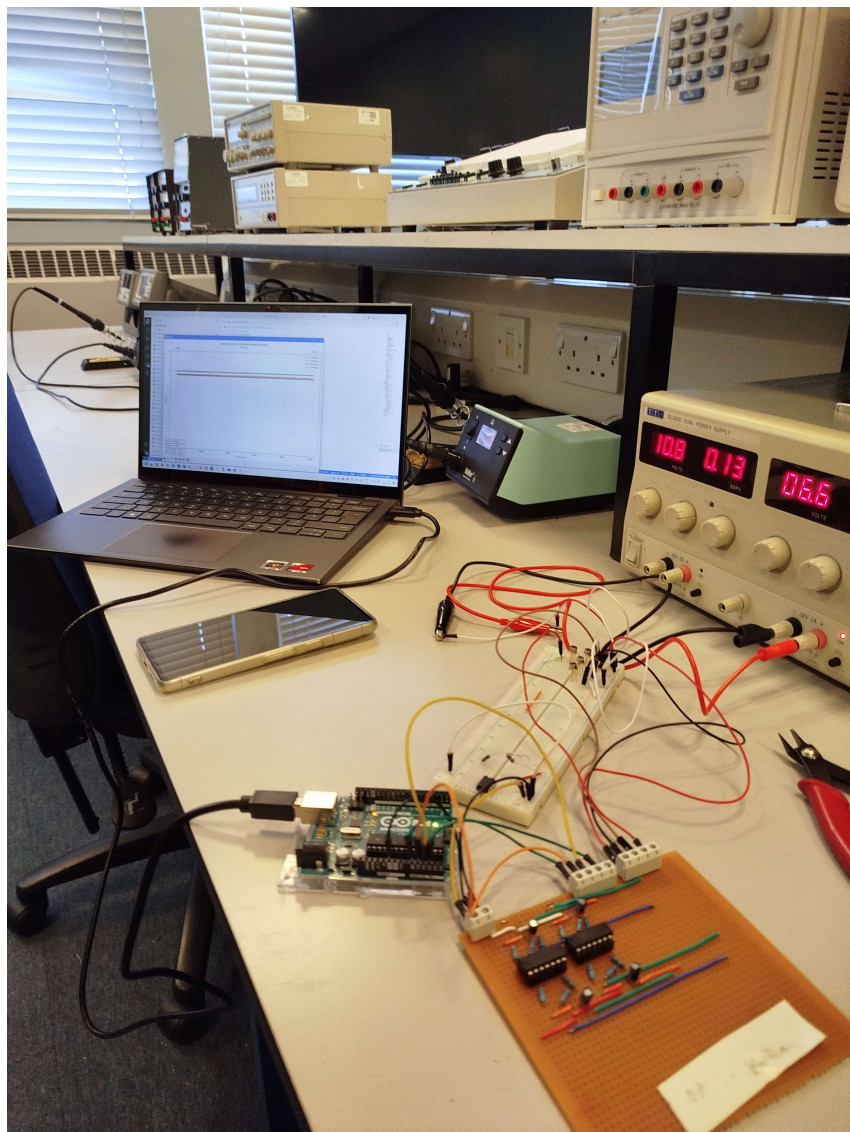
C.1.5. Solar Lab Prototype Testing



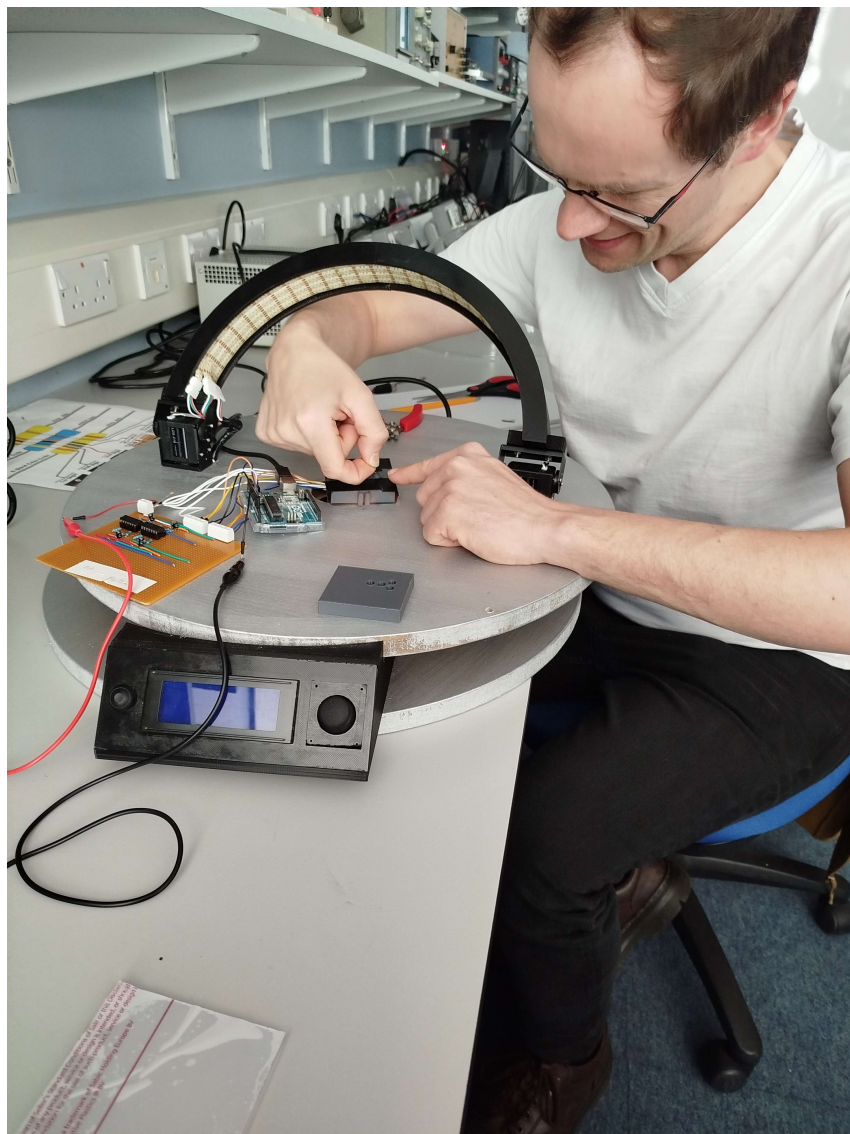
Lab Work for the Prototype (session 1)



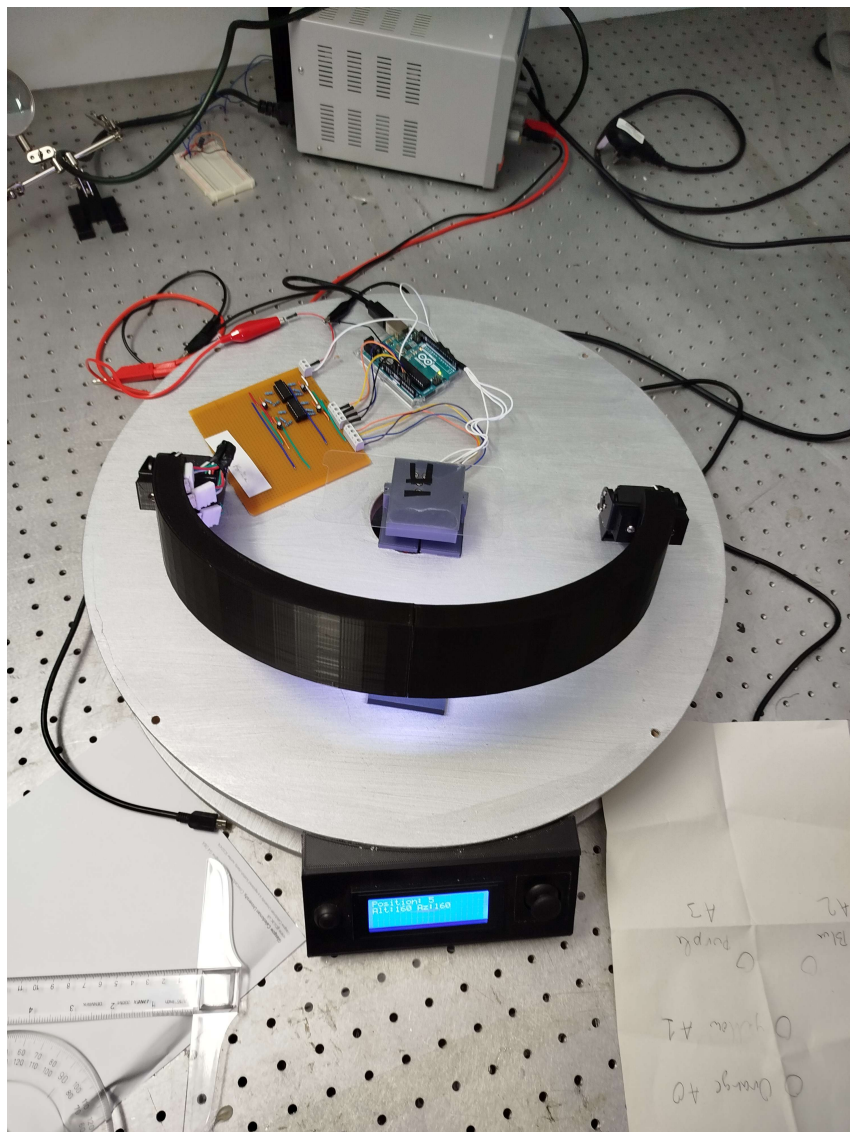
lab Work for the Prototype (session 2)



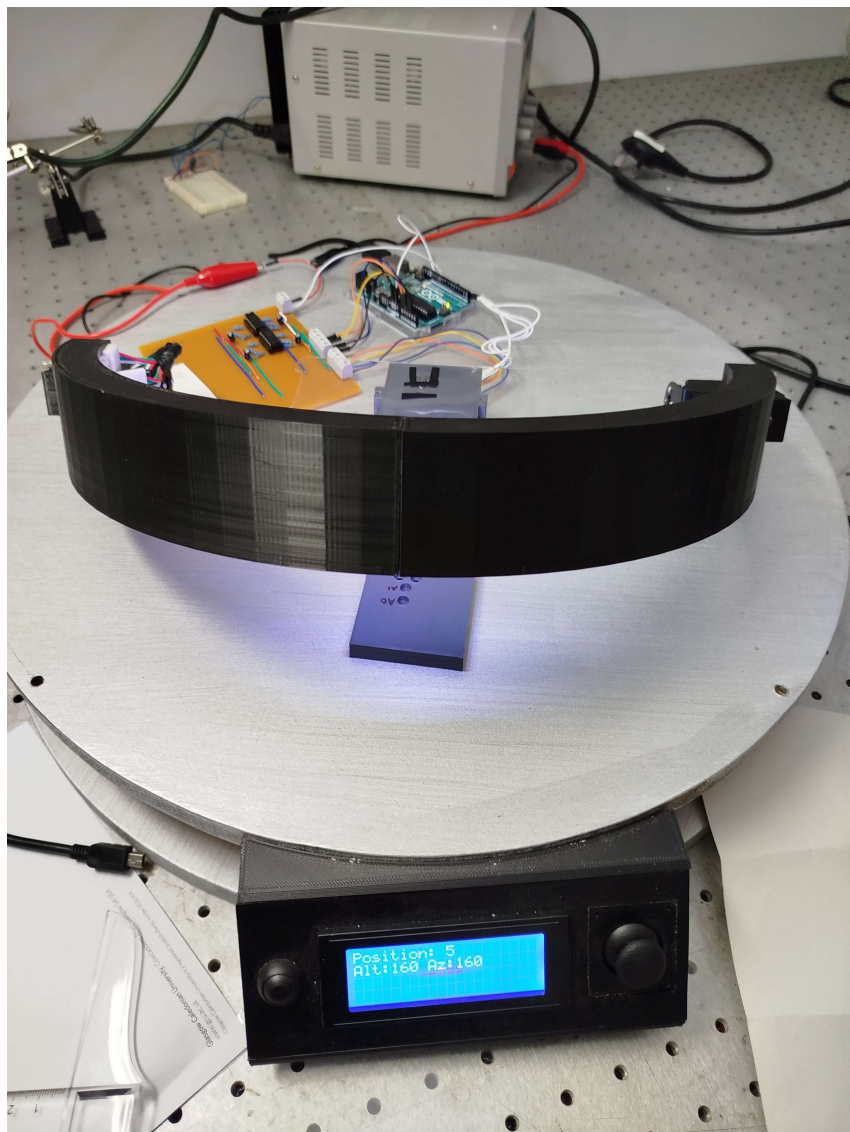
First Lab Test of the Prototype



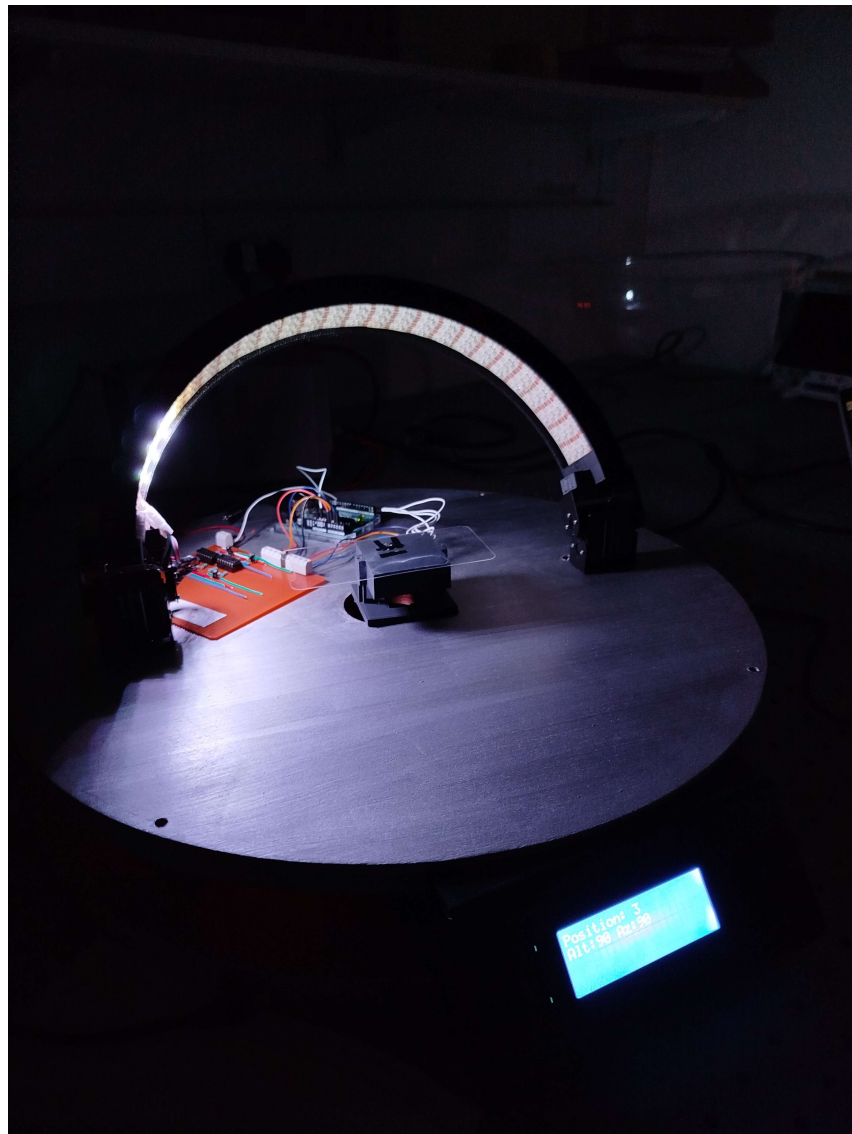
RED Testbench 1



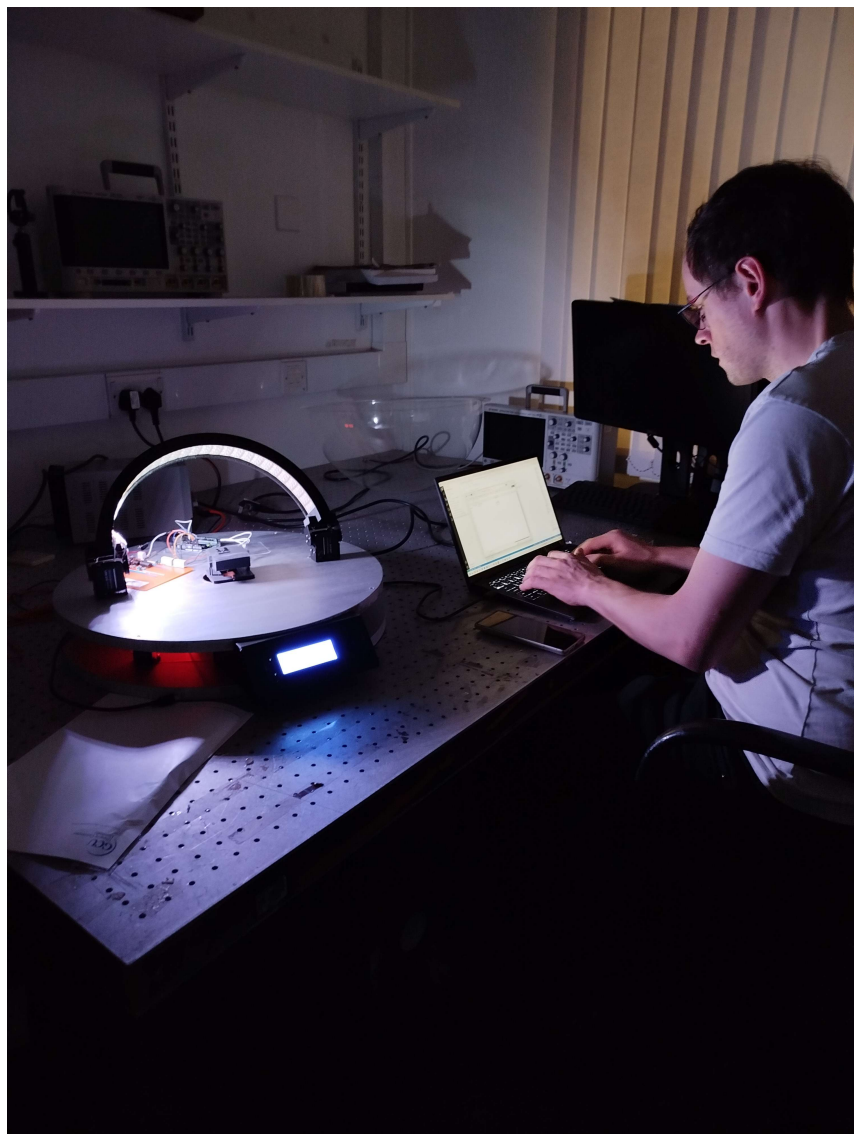
Solar Lab Test of the Prototype 1



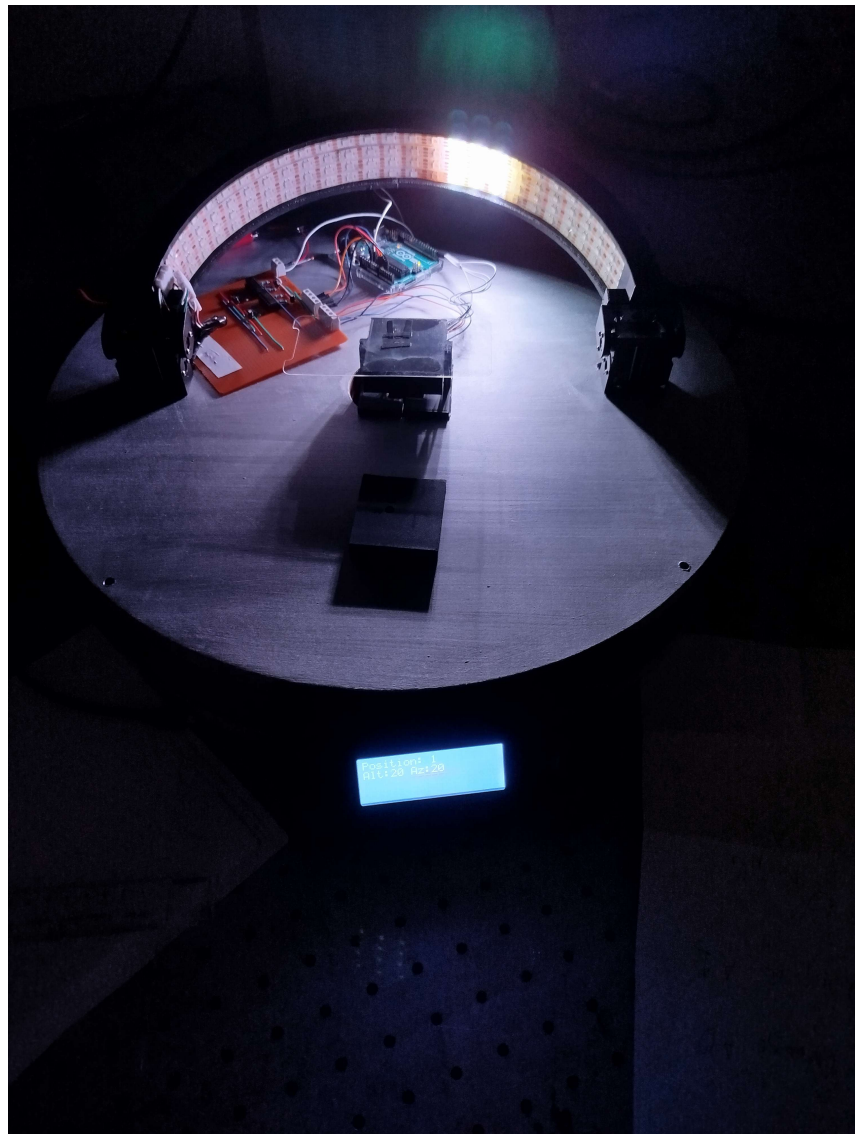
Solar Lab Test of the Prototype 2



Solar Lab Test of the Prototype 3



Solar Lab Test of the Prototype 4



Solar Lab Test of the Prototype 5

D. Appendix - Material Analysis

D.1. Section 1 Title

D.1.1. subsectiontitle

D.2. Section 2 Title

D.2.1. subsectiontitle